EURASIP Journal on Applied Signal Processing 2005:8, 1185–1204

Three-State Locally Adaptive Texture Preserving Filter for Radar and Optical Image Processing

Oleg V. Tsymbal
Kalmykov Center for Radiophysical Sensing of Earth NANU NSAU, 61070 Kharkov, Ukraine
Email: dmb@ire.kharkov.ua

Vladimir V. Lukin
Department of Transmitters, Receivers, and Signal Processing, National Aerospace University, 61070 Kharkov, Ukraine
Email: lukin@xai.kharkov.ua

Nikolay N. Ponomarenko
Department of Transmitters, Receivers, and Signal Processing, National Aerospace University, 61070 Kharkov, Ukraine
Email: uagames@mail.ru

Alexander A. Zelensky
Department of Transmitters, Receivers, and Signal Processing, National Aerospace University, 61070 Kharkov, Ukraine
Email: zelensky@xai.kharkov.ua

Karen O. Egiazarian
Institute of Signal Processing, Tampere University of Technology, 33101 Tampere, Finland
Email: karen@cs.tut.fi

Jaakko T. Astola
Institute of Signal Processing, Tampere University of Technology, 33101 Tampere, Finland
Email: jaakko.astola@tut.fi

Received 3 June 2004; Revised 11 October 2004; Recommended for Publication by Moon Gi Kang

Textural features are one of the most important types of useful information contained in images. In practice, these features are commonly masked by noise. Relatively little attention has been paid to texture preserving properties of noise attenuation methods. This stimulates solving the following tasks: (1) to analyze the texture preservation properties of various filters; and (2) to design image processing methods capable to preserve texture features well and to effectively reduce noise. This paper deals with examining texture feature preserving properties of different filters. The study is performed for a set of texture samples and different noise variances. The locally adaptive three-state schemes are proposed for which texture is considered as a particular class. For "detection" of texture regions, several classifiers are proposed and analyzed. As shown, an appropriate trade-off of the designed filter properties is provided. This is demonstrated quantitatively for artificial test images and is confirmed visually for real-life images.

Keywords and phrases: texture feature preservation, image processing.

1. INTRODUCTION

Texture features are widely used in image analysis and recognition [1]. This relates to remote sensing applications including microwave, optical, infrared, and multispectral where texture plays an important role in desired scene-type detection and localization, image classification, object discrimination and terrain delimitation, and so forth [2, 3, 4, 5]. The same concerns modern techniques of color image analysis, segmentation, and image retrieval from data bases [6, 7].

However, remote sensing images acquired from airborne or spaceborne carriers as well as images registered by video cameras and other sensors are commonly corrupted by noise. For optical and infrared images it is commonly assumed that the dominant noise is additive and its probability density function (pdf) is close to Gaussian [8]. For microwave radar

imagery the prevailing influence of multiplicative noise is typical and its pdf can be either close to Gaussian or essentially non-Gaussian depending upon the radar type and its characteristics [2, 5, 9, 10, 11]. This noise is commonly rather intensive and clearly observed visually in microwave images.

Noise presence causes problems in information retrieval from grey-scale and color images as well as from radar remote sensing data. Noise masks texture, distorts the textural feature parameter estimates obtained from noisy data, makes it more complex to solve the tasks of texture region detection, identification, discrimination, and so forth.

Because of noise, image filtering is a generally used operation in remote sensing data processing. It serves the goals of image enhancement, denoising and, as a result, improvement of data interpretation, classification, segmentation, and sensed terrain (scene) parameter estimation [9, 10, 11]. Although a large number of books and papers deal with image filtering, not many of them pay particular attention to texture preservation. To name a few, we mention the papers of Yunhan et al. [10], Aiazzi et al. [12], as well as the book of Perry et al. [13] (see also references therein). Preliminary results of the current paper have been published in [14, 15]. The analysis here is more thorough and extended in many respects, one of the most important of which is additionally studied additive noise case.

The paper [10] contains the performance comparison for a rather limited set of filters although it clearly demonstrates the difference in texture preservation for such typical scanning window filters as the standard mean and median [8], the local statistic Lee [16], and the sigma [17] filters. The two latter ones are shown [10] to preserve texture well enough. The conclusions given in [10] coincide with the ones presented in our work [14], where the modified sigma filter [18] is also considered.

The paper [12] deals with multitemporal remote sensing data and their applications. Similarly to the data presented in [11, 19], Aiazzi et al. underlines that small local variations of true image values that correspond to radar cross-section variations induced by local heterogeneity of surface backscattering should be preserved after image filtering; and these variations can be considered as texture.

Many other papers relating to image filtering either mainly deal with mosaic images or consider the texture in images under study as edges, details, and their neighborhoods (see, e.g., [20, 21, 22]). Although some concentration of details and some texture can visually have similar appearance, they, as it will be shown below, are not the same in the sense of filter performance assessment and filter selection. Simultaneously, texture and noise are also not the same from the viewpoint of local spatial correlation properties. Perry et al. [13] stress that "the textures usually have noise-like appearance although they are distinctly different from noise in that there exists certain discernible patterns within them." Here we can also add that while texture contains useful information the noise does not.

Recall that texture features are not the only class of useful information to be retrieved from images. For efficient filtering, it is also desirable to considerably suppress noise in image homogeneous (smooth) regions and to preserve edges and details. From these viewpoints, effective image processing can be provided by hard-switching locally adaptive filters [20, 21, 22, 23, 24]. The simplest versions of such filters that can be referred to as two-component or two-state ones [22] consist of a so-called noise suppressing filter (the standard mean, Wilcoxon, α-trimmed, etc. [8, 20, 22]) and a detail preserving filter (the local statistic Lee [16], the standard or modified sigma filters [17, 18], etc.).

The two-state locally adaptive filter (LAF) output is assigned to the output of either noise suppressing filter (NSF) or detail preserving filter (DPF). This hard switching is performed according to the results of comparing the local activity indicator (LAI) to the predetermined threshold. As LAI, the local statistical parameters like local variance, quasirange, trimmed local variance, and so forth, calculated for given scanning window, are used [20, 22]. If the dominant type of noise is multiplicative, then these local statistic parameters are to be normalized [20, 22, 23].

For two-state LAFs many image texture regions are classified to "locally active areas" and, thus, they are processed by the detail preserving filter (DPF). In general, DPFs [16, 17, 18] preserve texture features not badly [10, 14]. However, they are not the best choice for processing texture regions. Thus, three problems arise. First, what is the best filter in the sense of texture feature preservation? Second, if there exists such a filter and it is not the same as the best DPF, then, can this filter be incorporated in the structure of the locally adaptive hard switching filters? The third question is how to detect and localize the texture regions?

In this sense, one should keep in mind that our intention is not to detect one or few particular texture types as in some applications [3, 4] but to localize the areas with different types of texture characterized by various statistical and/or spatial correlation parameters.

It is worth noting here that more sophisticated versions of locally adaptive filters (with larger number of used component filters and with more complex methods of analysis of image local behavior) [24, 25] are unable to effectively solve the above-mentioned problems since (a) the first question has not been answered there anyway; (b) texture has not been considered as particular class and it could not be so. The reason is that image "local analysis" has been performed in the scanning window of size 5×5 pixels [24, 25]. At the same time, texture elements generally have larger size and, thus, the sliding windows used in texture analysis and parameter estimation commonly have the size 12×12 or 16×16 pixels [3].

These were the reasons for our decision to modify the hard switching two-state locally adaptive filter to the three-state one [14, 15]. The proposed filter had the states corresponding to the three classes: image homogeneous regions, edges and details, and texture regions. The local statistic Lee filter [16] was proposed in [14] for application in texture regions. It performed quite well, but later it has been shown that the local statistic Lee filter was not the best choice [15]. DCT-based filter performs considerably better [15]. This will be confirmed in Section 3.

It stems from the theory of hard-switching locally adaptive filters [20, 22, 24] that their performance depends upon the selection of component filters. Therefore, for a three-state LAF under design, its performance should depend upon selection of NSF, DPF, and texture preserving filter (TPF). The properties of hard-switching LAFs also depend upon the reliability of image pixel preclassification, that is, their referring to the corresponding classes.

Such preclassification should successfully solve this task for different levels (variances) and types of noise. We suppose that noise type is either known a priori or predetermined using the corresponding methods, for example, those ones proposed by Carton-Vandecandelaere et al. [26]. Then, the statistical parameters of noise can also be estimated [27, 28]. They can be also known a priori. After this, it becomes possible to separately consider the cases of dominant influence of multiplicative or additive noise, and this is done in Sections 4 and 5, respectively. Numerical simulation data are presented in Sections 3, 4, and 5 while real image processing examples are given in Section 6.

2. IMAGE/NOISE MODELS

The noise characteristics of remote sensing (RS) and other kinds of images depend upon different factors [22]. Nevertheless, the simplified universal one-channel RS image model can be represented as follows:

$$I_{ij} = \begin{cases} \mu_{ij} \cdot I_{ij}^{\text{true}} + n_{ij} & \text{with probability } 1 - P_{\text{imp}}, \\ A_{\text{imp}} & \text{with probability } P_{\text{imp}}, \end{cases} \quad (1)$$

where I_{ij} is the ijth noisy image sample value, I_{ij}^{true} is the true image value for the ijth sample, μ_{ij} is a stochastic variable that denotes multiplicative noise (with $\langle \mu \rangle = 1$ and the relative variance σ_μ^2), n_{ij} is the additive noise component with zero mean and variance σ_n^2. A_{imp} is a value of an image pixel corrupted by impulse spike (or burst) that can be encountered in image sample with probability P_{imp}.

Further, we consider impulse-free images since all impulse noise and bursts can be removed at the preliminary stage of RS image processing. This can be done using the preprocessing methods proposed by us in [29, 30].

As was mentioned in the Introduction, in this paper we consider two basic cases: the dominant influence of multiplicative (speckle) or additive noise. The situation where an image is corrupted by the former type of noise is considered in this paper in more detail compared to [15].

Multiplicative noise is typical for radar and ultrasound imaging systems [22]. The noise characteristics in radar images depend upon several factors like system type (synthetic aperture radar (SAR) or side look aperture radar (SLAR)) and SAR parameters (one-look or multilook, etc.). The simplified radar image models commonly take into account the multiplicative noise only, and can be described as follows [22]:

$$I_{ij} = I_{ij}^{\text{true}} \cdot \mu_{ij}. \quad (2)$$

For the simplified model (2) the influence of radar point spread function and additive noise is neglected. In most real cases μ_{ij} can be considered as having invariable properties for an entire radar image ($\sigma_\mu^2 = \text{Const}$). Typical values of σ_μ^2 are of the order $0.004, \ldots, 0.02$ for SLAR images and slightly larger for multilook SAR images [22].

The basic attention in this paper is paid to the case when the image is formed by SLAR or by multilook SAR with rather large number of looks. Therefore, it can be supposed that the multiplicative noise pdf is close to Gaussian [22]. However, it is demonstrated in Section 6 that the proposed approach is also applicable to processing radar images corrupted by nonsymmetric pdf speckle (SARs) if the corresponding prefiltering of such images has been carried out.

Another important aspect that we try to stress in this paper is the case of prevailing additive noise. For example, for a wide class of optical images the simplified observation model is [8]

$$I_{ij} = I_{ij}^{\text{true}} + n_{ij}. \quad (3)$$

Additive noise n_{ij} is supposed Gaussian and this assumption is valid for many practical applications [8, 9, 13]. Also, assume additive noise variance σ_n^2 is a constant value for entire image ($\sigma_n^2 = \text{Const}$).

In our simulations we consider i.i.d. (spatially uncorrelated) multiplicative and additive noise. Although this is not always true in practice (especially, for radar imaging), this paper is only the first step in design of efficient texture preserving techniques and, thus, we restricted ourselves considering i.i.d. noise with planning to study spatially correlated noise cases in future.

3. STUDY OF TEXTURE FEATURE PRESERVATION BY DIFFERENT FILTERS

We first perform property analysis of different filters in the sense of texture preservation. Thorough study of such properties for a very wide variety of filters is impossible because of several reasons. First, texture can be characterized and described in different ways using various sets and combinations of parameters [1, 31, 32, 33]. Really, many different approaches involving random Gaussian and Markov field models, fractals, orthogonal transforms, and so forth, are applied to texture modeling nowadays (see [34] and references therein). Second, while analyzing texture feature preserving performance of filters one should keep in mind what will be the further goal of prefiltered image processing (e.g., texture discrimination, parameter evaluation, etc.) and what technique will be applied. Since we do not know the goal of further image processing in advance, it has been decided to consider several typical characteristics and parameters of different texture regions for noise-free images, noisy ones, and the images after filtering.

In particular, quite often the higher-order statistics (moments) of texture region pdf estimations are used [1, 31, 32]. Thus, below we analyze the texture region mean, the

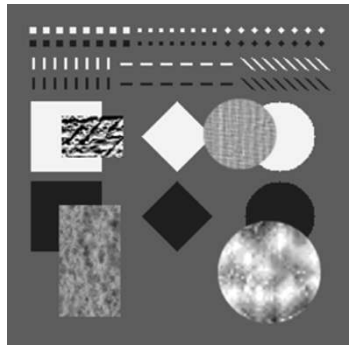

Figure 1: The noise-free test image (256 × 256) with four texture regions.

variance σ^2, the skewness ξ, and the kurtosis ψ (normalized σ^2 was used and it was calculated as $\sigma^2 = (1/|G_{\text{text}}|)\sum_{ij\in G_{\text{text}}}(I_{ij}-\overline{I}_{G_{\text{text}}})^2/(\overline{I}_{G_{\text{text}}})^2$, where $\overline{I}_{G_{\text{text}}}$ denotes the local mean determined for entire texture region G_{text}, $|G_{\text{text}}|$ is the number of pixels that belong to this region). Note that the noise present in an image can rather considerably change these statistics in comparison to the noise-free texture (see data presented in Figure 2). Another approach assumes the analysis of spatial spectrum or correlation characteristics [1, 5, 33] that are connected with cooccurrence matrix-based methods for texture recognition. So, we also consider the basic parameters of spatial autocorrelation function (ACF) like the main lobe width, maximal side lobe level, its visual appearance, and so forth. Besides, some people are more used to analyze the filter performance in terms of mean square error (MSE) or peak signal-to-noise ratio (PSNR) although these are not the best criterions from the viewpoint of processed image quality evaluation [13]. Nevertheless, the integral and local PSNR values have been calculated for entire test image in Figure 1 and for its fragments.

Analysis has been performed for the four types of texture that had rather different properties. The first texture type is an intensive medium-grain texture (rectangular shape fragment in the left-top part of the test noise-free image in Figure 1, this texture is called "Cement"). The second type called "Linen" is nonintensive small-grain texture (the circular shape fragment in the right-top part). The third sample of texture "Bread" is the large rectangular object in left-bottom part, it can be classified as medium-intensity medium-grain texture. Finally, the fourth texture sample (large-circle shape fragment in the right-bottom part, called "Cracks") can be classified as medium-intensity large-grain texture. As seen from Figure 1, beside the aforementioned texture regions (TR), the test image also contains homogeneous regions (HR) and edge/detail neighborhood regions (EDNR).

The study of texture feature preserving properties has been performed for a rather wide set of different filters that belong to NSF and DPF classes. As representatives of NSF class, the standard mean (*mean*), median (*median*), and the L_{pq}-NSF also called the sum-rank filter (*sum.rank*) [22, 23] have been exploited. The set of the considered DPFs has included the following filters. First, the standard sigma (*Sigma*) [17], the local statistic Lee (*Lee*) [16], the center-weighted median (*CWMF*) [8] with different weights, and the FIR median hybrid filters (modification 3*L*+ [35]) (*FMHF*) have been studied. For the two latter filters the scanning window was 5×5, whilst for the standard sigma and Lee filters it varied from 3×3 to 9×9 pixels. Second, the modified sigma filters (*MSF*) have been exploited for the cases of dominant multiplicative [18] and additive [36] noise. Their scanning window size also varied. Besides, for the standard and modified sigma filters as well as for the local statistic Lee filter, we used as the input parameters not only the true values of σ_μ^2 (or σ_n^2) but also slightly smaller and larger values (they are presented in Table 1). Third, we have also analyzed the filtering method based on spatially invariant discrete cosine transform (DCT) [37, 38].

Typically, the transform-based methods are intended for application in additive Gaussian noise environment [37, 38, 39]. However, recently there were quite many attempts to modify these methods to make them applicable to processing the images corrupted by multiplicative (even speckle) noise [37, 38, 40]. One of the possibilities is to apply at the first stage the direct logarithmic transform $I_{ij}^h = [a\log_b(I_{ij})]$, where a and b are some parameters, $[\cdot]$ denotes the rounding-off operation. Our investigations have shown that if an original radar image is represented as 8-bit 2D data array, the best choice to get 8-bit image representation after direct homomorphic transform and to ensure minimal distortions due to rounding-off errors is to use $a = 8.39$ and $b = 1.2$. Then, the spatially invariant DCT filtering is to be applied followed by the corresponding inverse homomorphic transform. After the aforementioned direct homomorphic transform, Gaussian multiplicative noise in original radar image converts to additive quasi-Gaussian noise with variance σ_{add}^2 recalculated as $\sigma_{\text{add}}^2 = a^2\sigma_\mu^2/(\ln b)^2$.

The hard-threshold DCT-based filtering presumes assigning zero values to those DCT spectral coefficients that do not exceed the predetermined threshold. This threshold is commonly set proportional to noise standard deviation where the recommendations are to use the factors within the limits from 2 to 4 [39]. According to the results we have obtained by analyzing several textures and noise variances, our recommendation is to set the threshold t_{DCT} twice larger than the noise standard deviation σ_{add}. Note that if the noise in an image is additive, then the operations of direct and inverse homomorphic transform are unnecessary, and $t_{\text{DCT}} = 2\sigma_n$. The scanning window size for DCT-based filtering was 8×8 pixels although for the 16×16 window the filter performance was almost the same.

As can be predicted and follows from previous analysis [10, 14, 15], all filters referred to NSF class severely degrade texture features. All NSFs radically change the variance σ^2, the skewness ξ, and the kurtosis ψ with respect to the initial values for the corresponding fragments of the noise-free test image (see Figure 2). If NSF scanning window size increases (see the plots for the mean, median, and sum-rank filters in Figure 2), the differences between original values of σ^2, ξ, and ψ (*original*) and their estimates obtained for processed images, as a rule, increase.

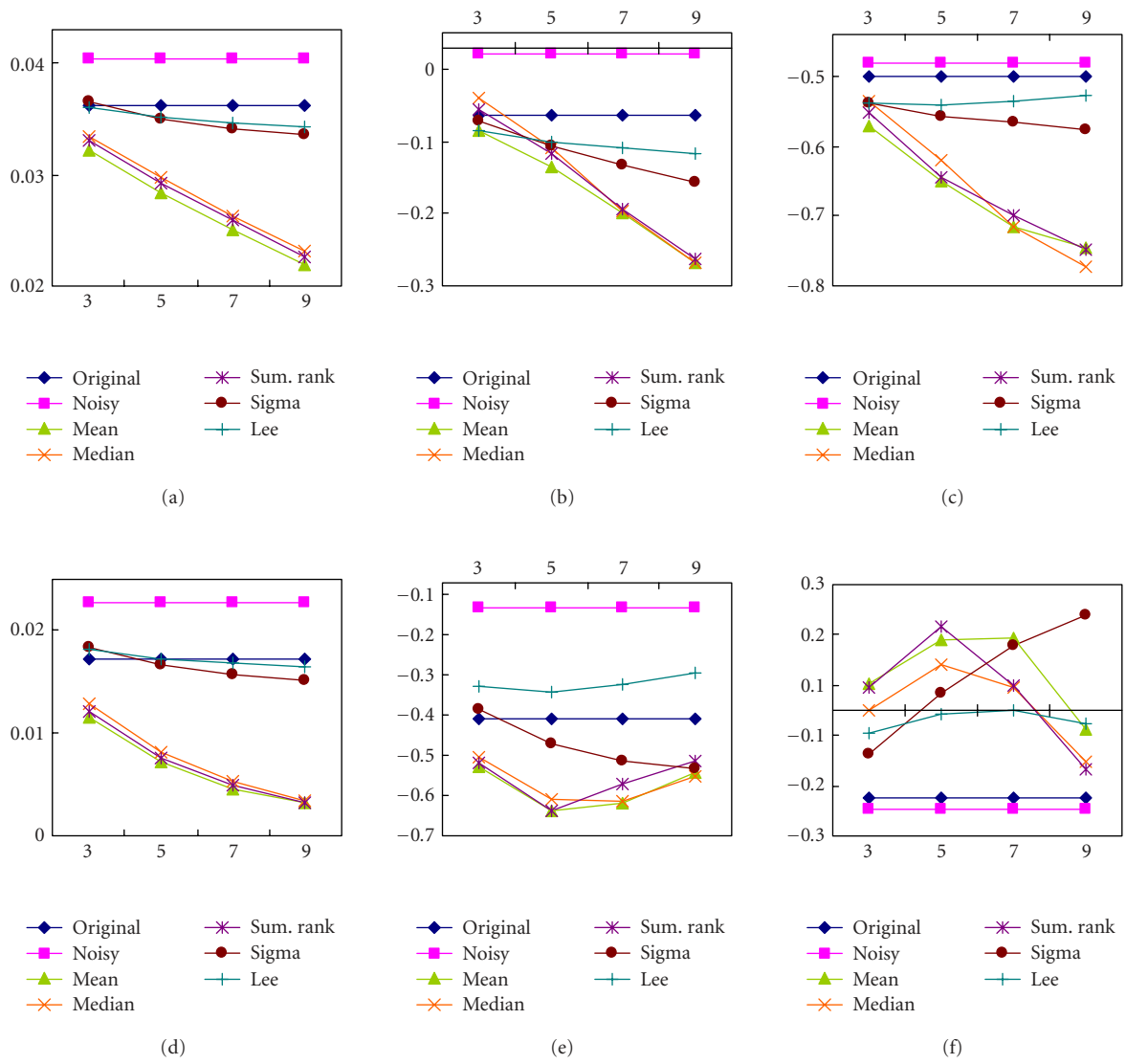

Figure 2: Diagrams of statistical characteristics (vertical axis): (a), (d) the relative local variance, (b), (e) the skewness, and (c), (f) the kurtosis of the textural fragment in the right bottom part ((a) , (b), and (c)) and in the left bottom part ((d), (e), and (f)) of the test image (Figure 1) corrupted by Gaussian multiplicative noise ($\sigma_\mu^2 = 0.005$) depending on the square sliding window side size (horizontal axis).

Besides, the image texture regions processing by NSF leads to a considerable change in basic characteristics of 2D ACF (compare the ACF in Figure 3a to ACFs in Figures 3c, 3d, and 3e; also compare the ACF in Figure 4a to the ACF in Figure 4c). In particular, after processing by NSF the ACF main lobe becomes wider; the side lobes are substantially smeared, and so forth. The destructive influence of NSF application on texture regions will be also clearly seen from the data presented in Table 2 for the 7×7 L_{pq}-filter where in the rightmost column the values of local MSE and PSNR are given for all texture regions of the test image (in aggregate). Note that all aforementioned effects have been observed for both multiplicative noise variances $\sigma_\mu^2 = 0.005$ and $\sigma_\mu^2 = 0.012$ and for all four considered textures.

In turn, the filters referring to the class of DPFs perform texture feature preservation much better than any NSF. After DPF application the values σ^2, ξ, and ψ usually become closer to initial values for noise-free texture regions than they were for noisy images. The effect of scanning window size for DPFs is also not as crucial as for NSFs. This is clearly seen for the standard sigma and Lee filters used as examples of DPFs in Figure 2. Besides, as seen in Figures 3f, 3g, and 3h, the 2D ACFs are much closer to the ACF in Figure 3a than the ACFs for outputs of NSFs (Figures 3c, 3d, and 3e). The analysis of 2D ACFs in Figures 4d and 4e also shows that they are much more similar to the ACF in Figure 4a than the ACF for the median filter output (Figure 4c).

For the DCT-based filter for the texture region Cracks, the obtained σ^2, ξ, and ψ are equal to 0.035, -0.144, and -0.56, respectively. Comparing them to the data presented in Figure 2, we can assure that they are quite close to original ones and approximately at the same level as for the

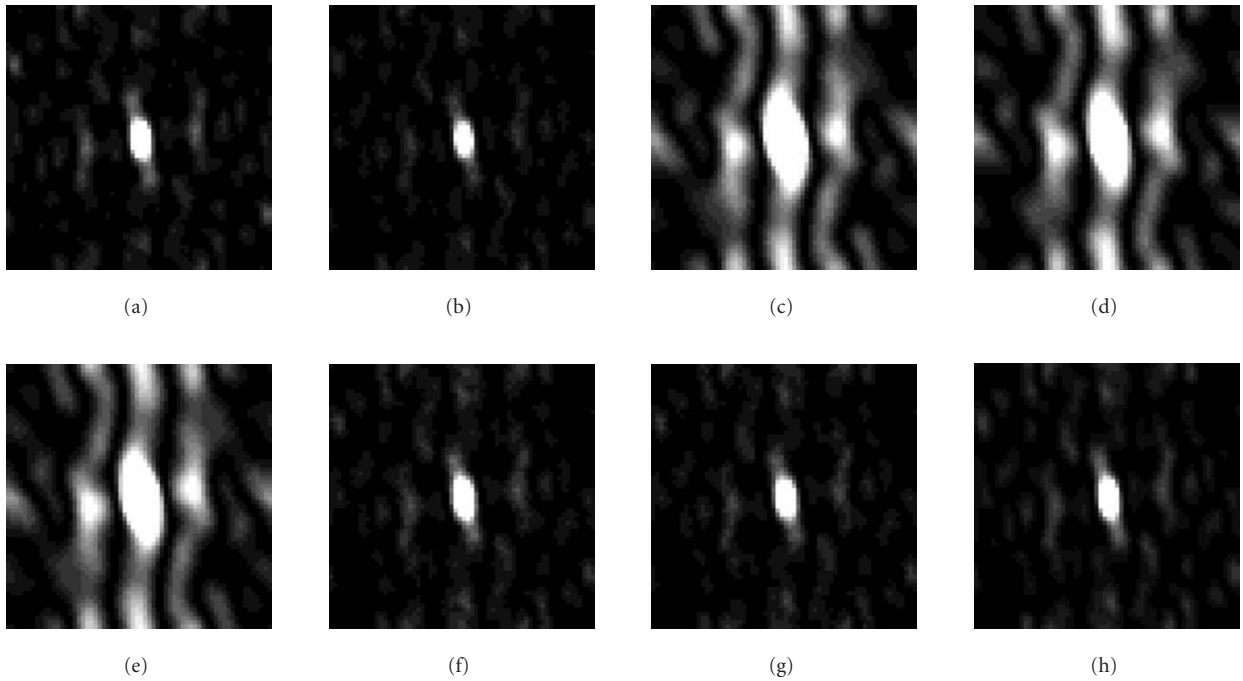

Figure 3: Two-dimensional grey-scale representation of 64×64 ACFs for the left-bottom texture fragment of (a) the noise-free test image, (b) the test image corrupted by Gaussian multiplicative noise ($\sigma_\mu^2 = 0.005$), and the same image processed by (c) 7×7 mean, (d) 7×7 median, (e) 7×7 L_{pq}, (f) 7×7 Sigma, (g) 7×7 local statistic Lee, and (h) 8×8 DCT-based filters. (The dynamic diapasons of 2D-ACFs representation are identically corrected for better visual perception.)

local statistic Lee filter. It is also seen from analysis of ACFs in Figures 3h and 4f that the DCT-based filter practically does not distort the 2D ACF of texture samples.

The analysis and comparisons performed above have been done for particular textures and for given values of σ_μ^2. In order to prove that the obtained dependencies and conclusions are valid for different textures and noise properties, we consider additional simulation data.

As another possible approach, the comparison of texture preserving properties of filters has been also performed using the plots of texture region skewness and kurtosis represented as the corresponding points on plane (see Figure 5). This figure shows few examples for both $\sigma_\mu^2 = 0.005$ and $\sigma_\mu^2 = 0.012$ that correspond to typical levels of multiplicative noise in SLAR images.

Numerical results for one more texture sample (right top) that have not been shown in Figure 5 can be found in Table 1.

The obtained plots allow to analyze in what degree the skewness and kurtosis are changed after (due to) filtering and to compare the obtained values to original (noise-free) ones. As seen, the considered Lee and DCT filters that belong to DPF class do not change the higher-order statistics too much. For some types of textures practically ideal preservation of texture higher-order statistics is provided by one group of filters. An example is the high-contrast left-top texture (see Figures 5c and 5f) for which the DCT-based and the 5×5 and 7×7 local statistic Lee produce practically "perfect match." However, it can be seen that in many cases the FMHF and sometimes CWMF (with the central weight 11) provide good results as well. Nevertheless, their PSNR results (see Table 1) are far from the best.

Additional data that characterize texture feature preserving properties of different filters for the four considered texture types are presented in Table 1 for $\sigma_\mu^2 = 0.005$ and $\sigma_\mu^2 = 0.012$ cases.

As seen, in aggregate, the best results have been provided by the local statistic Lee (5×5 and 7×7) and the proposed version of the DCT-based technique. For them the values of skewness and kurtosis for all four textures differ from the true values by no more than 0.2 (see also Figure 5) while for other filters like MSF or CWMF radical changes of these texture features have been observed. Besides, the Lee and DCT-based filters produce PSNRs that are the largest among all considered filters (i.e., the corresponding values of MSE are the smallest) for all four textures. Note, that the best results are provided by an 8×8 or 9×9 DCT filter. Since the advantage of the latter is not essential, the use of more computationally attractive 8×8 DCT variant is preferable. The preponderance of DCT filter is also clearly demonstrated by visual filtering results of texture samples in Figure 6.

Excellent texture preserving properties of the DCT-based filter can be easily explained and they stem from principles of transform-based filtering [38, 39]. If the processed texture has some specific spatial spectral harmonics, then with high probability they will remain unchanged (since they exceed the hard threshold) after assigning zero values to some percentage of spectral coefficients which, most likely,

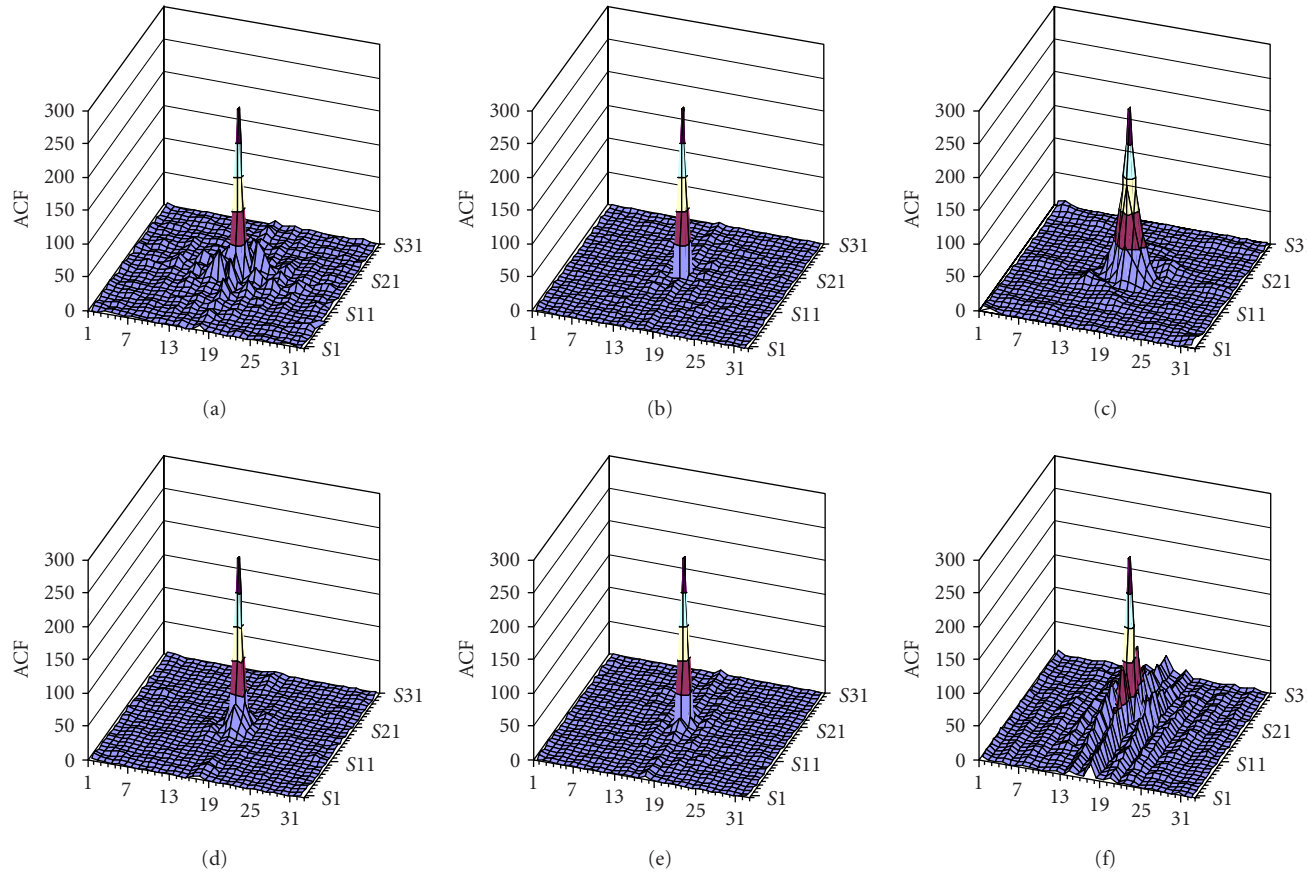

Figure 4: Three-dimensional representation of the right-upper texture fragment ACF (32×32): (a) noise-free, (b) corrupted by Gaussian multiplicative noise with $\sigma_\mu^2 = 0.012$, and after processing the image by (c) the 5×5 median filter, (d) the 5×5 modified sigma filter, (e) the 5×5 local statistic Lee filter, and (f) the 8×8 DCT-based filter.

correspond to noise. Thus, the texture, irrespective of its spatial spectral characteristics, is preserved well and noise is effectively suppressed.

The data presented in Table 1 one more time underlines the problems of texture region filtering. For some textures like the right-bottom and right-top ones the 4–6 dB PSNR increasing is provided by the best filters and the application of all the considered filters leads to PSNR improving. At the same time, for the left-top texture, practically no improvement is ensured even by the best filters. Moreover, the application of some filters results in even considerable decreasing of PSNR. This takes place, for instance, for the CWMF (see Table 1).

The aggregate PSNR and MSE values calculated for all four texture regions together are given in Table 2 in the rightmost column. Due to the DCT-based filter application, the PSNR values have been improved (increased) by 4-5 dB. The PSNRs for the DCT-based technique are, at least, by $1 - 2$ dB better than for any other DPF for both $\sigma_\mu^2 = 0.005$ and $\sigma_\mu^2 = 0.012$.

The final argument that gives additional information to quantitative analysis performed above is visual analysis of texture processing. The visual analysis still remains the key factor from which one can make conclusions concerning filter quality and conceive the entire explicit numerical results for the considered filters.

The visual results of processing the considered texture samples by some of the studied DPFs are presented in Figure 6. As can be seen, the 5×5 CWMF with the central element weight 11 that provides the best PSNR results among CWMFs does not show good enough texture preservation (Figure 6c); besides, rather intensive residual noise is noticeable. The FMHF that retains high-order statistics well possesses, probably, the worst noise suppression among the studied techniques (see Figure 6d). This fact is also confirmed by the corresponding PSNR values that are rather low (see Table 1). Among sigma filters, the application of MSF even if scanning window is rather small (5×5) results in noticeable detail smearing (Figure 6f) compared to its conventional version (Figure 6e). For the latter case, noise reduction is not appropriate. Nevertheless, from Figure 6f one can see the MSF tendency to emphasize the edges of small homogeneous object that is very useful in such class of tasks.

The best overall ability to preserve texture simultaneously with noise suppression is provided by local statistic Lee filter (Figure 6g) and DCT-based filter (Figure 6h).

All this shows that the DCT-based filtering can be very useful for texture feature preservation and it can be

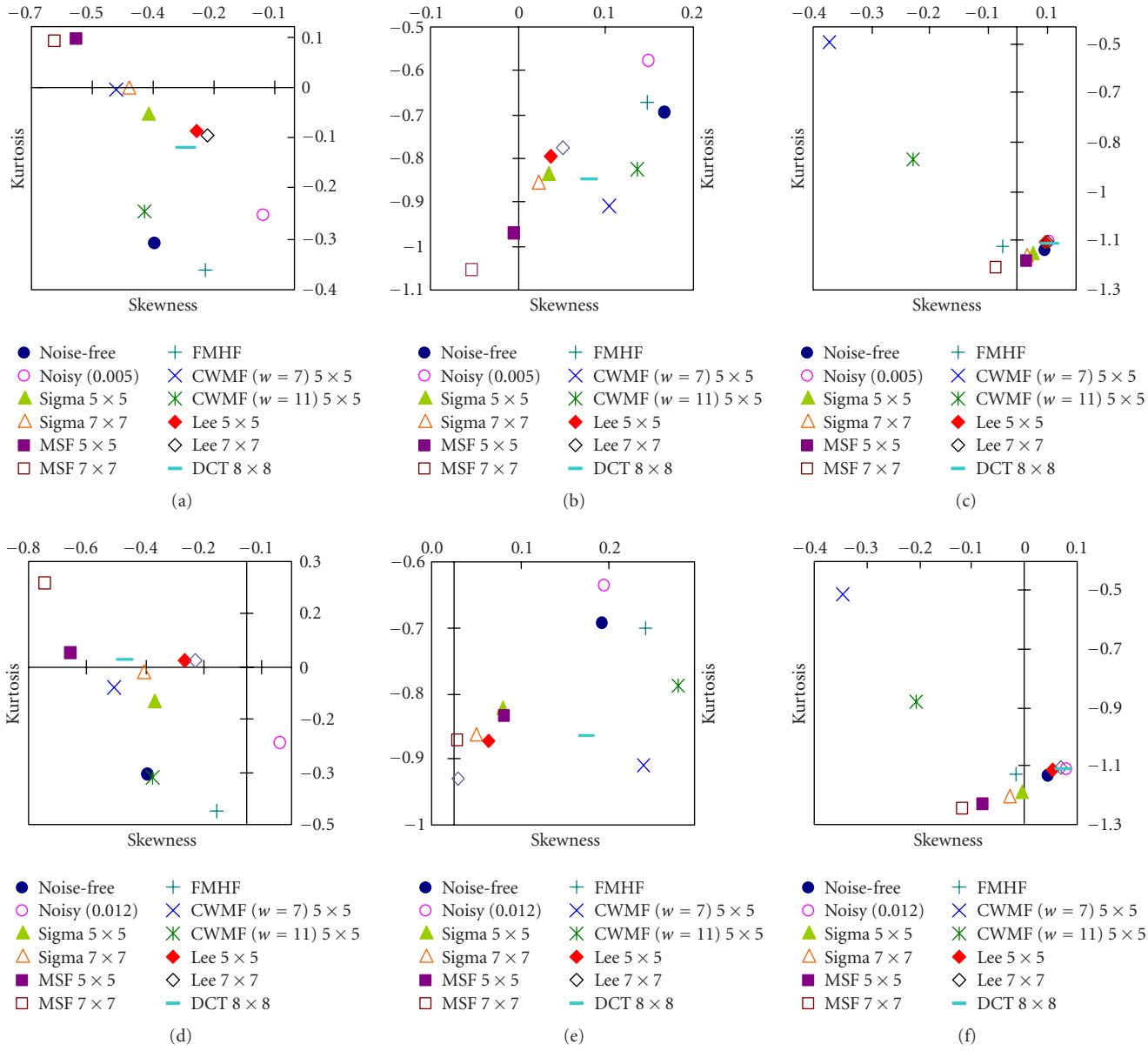

FIGURE 5: Joint graphical representation of kurtosis and skewness for original and noisy textures and these textures are processed by different detail preserving filters: (a), (d) left-bottom, (b), (e) right-bottom, and (c), (f) left-top textures in Figure 1, corrupted by Gaussian multiplicative noise: (a), (b), (c) with $\sigma_\mu^2 = 0.005$ and (d), (e), (f) with $\sigma_\mu^2 = 0.012$.

recommended as the best component filter for the three-state locally adaptive hard-switching scheme under design.

As can also be seen from Table 2, the DCT-based filtering does not outperform the 7×7 L_{pq}-filter in image homogeneous regions. In turn, the L_{pq}-filter produces severe distortions in texture regions. In edge/detail regions and their neighborhoods the best local MSE and PSNR values are provided by the modified sigma filter. This allows expecting that if the image homogeneous regions, the edge/detail neighborhoods, and the texture regions would be reliably classified, the locally adaptive hard-switching filtering could ensure the desirable trade-off of image processing properties.

4. PROPOSED THREE-STATE LOCALLY ADAPTIVE FILTER FOR MULTIPLICATIVE NOISE CASE

Recall that the two-state locally adaptive filter output is defined as [20, 22, 23]

$$I_{ij}^{f} = \begin{cases} I_{ij}^{\mathrm{NSF}}, & S_{ij}^{2\mathrm{st}} = 1, \\ I_{ij}^{\mathrm{DPF}}, & S_{ij}^{2\mathrm{st}} = 2, \end{cases} \quad S_{ij}^{2\mathrm{st}} = S_{ij}^{1\mathrm{thr}} = \begin{cases} 1, & \vartheta_{ij} \le \vartheta_t, \\ 2, & \vartheta_{ij} > \vartheta_t, \end{cases} \tag{4}$$

where I_{ij}^{NSF}, I_{ij}^{DPF} are the outputs of the used NSF and DPF, respectively; $S_{ij}^{1\mathrm{thr}}$ denotes the one-threshold preclassifier (PC) used in this case as the two-state PC ($S_{ij}^{2\mathrm{st}}$), ϑ_{ij} is the LAI value, ϑ_t defines the threshold. If $\vartheta_{ij} \le \vartheta_t$, the pixel

Table 1: Comparative quantitative results of application of different DPFs to four texture samples corrupted by multiplicative Gaussian noise with $\sigma_\mu^2 = 0.005$ and $\sigma_\mu^2 = 0.012$.

	Left-top texture (Cement)			Left-bottom texture (Bread)			Right-bottom texture (Cracks)			Right-top texture (Linen)				
	PSNR	MSE	σ^2	PSNR	MSE	σ^2	PSNR	MSE	σ^2	PSNR	MSE	σ^2	k	γ
Noise-free	—	—	0.463	—	—	0.020	—	—	0.027	—	—	0.007	0.154	0.236
Noisy ($\sigma_\mu^2 = 0.005$)	29.01	81.67	0.463	28.47	92.32	0.026	26.09	159.88	0.030	27.2	123.93	0.012	0.259	0.194
Sigma 5×5	28.41	93.89	0.458	29.99	65.13	0.019	28.9	83.75	0.024	29.1	79.93	0.006	0.239	2.293
Sigma 7×7	28.46	92.62	0.457	29.9	66.5	0.018	28.44	93.23	0.023	29.13	79.51	0.005	0.302	2.698
MSF 5×5	26.59	142.5	0.449	29.68	70.09	0.016	29.33	75.86	0.022	28.3	96.29	0.003	0.366	7.728
MSF 7×7	26.98	130.4	0.445	29.58	71.61	0.014	28.5	91.96	0.021	28.49	92.09	0.003	0.717	8.593
FMHF 5×5	24.84	213.4	0.420	29.48	73.36	0.021	27.22	123.42	0.027	28.47	92.79	0.007	0.235	−0.595
CWMF 5×5 ($w = 7$)	15.44	1857	0.224	29.09	80.16	0.013	28.93	83.17	0.021	27.74	109.37	0.002	0.606	0.361
CWMF 5×5 ($w = 9$)	16.94	1315	0.268	29.49	73.07	0.014	28.83	85.15	0.022	28.11	100.58	0.003	0.509	−0.057
CWMF 5×5 ($w = 11$)	18.45	930.2	0.310	29.72	69.33	0.016	28.52	91.41	0.023	28.36	94.91	0.003	0.429	−0.338
Lee 5×5	28.99	82.01	0.452	30.07	64.05	0.020	28.79	85.86	0.025	29.17	78.66	0.006	0.32	0.455
Lee 7×7	28.98	82.27	0.450	29.87	66.96	0.020	28.21	98.16	0.024	29.14	79.21	0.006	0.319	0.422
DCT 7×7	29.02	81.49	0.464	31.4	47.06	0.018	31.98	41.25	0.023	30.82	53.84	0.004	0.316	0.344
DCT 8×8	29.05	81.01	0.463	31.47	46.47	0.018	31.76	43.38	0.023	31	51.63	0.004	0.329	0.193
DCT 9×9	29	81.87	0.464	31.46	48.08	0.018	32.02	40.86	0.024	31.01	51.59	0.004	0.29	0.181
Noisy ($\sigma_\mu^2 = 0.012$)	25.08	201.9	0.472	24.92	209.6	0.036	22.55	361.3	0.036	23.6	284	0.019	0.329	0.224
Sigma 5×5	24.45	233.2	0.455	27.85	106.8	0.022	26.59	142.8	0.026	26,78	136.5	0.006	0.079	1.625
Sigma 7×7	24.51	230.4	0.451	27.68	111.1	0.020	26.23	155	0.025	26.93	131.8	0.005	−0.036	1.473
MSF 5×5	22.85	337.7	0.440	28.06	101.7	0.015	27.92	104.9	0.022	26.66	140.3	0.002	−0.098	1.762
MSF 7×7	23.04	323.2	0.431	27.75	109.2	0.014	27.05	128.3	0.020	26.99	130.1	0.002	0.158	0.335
FMHF 5×5	23.13	316.6	0.423	26.6	142.2	0.027	24.19	247.8	0.032	25.61	178.8	0.011	0.203	−0.503
CWMF 5×5 ($w = 7$)	15.29	1922	0.220	28.15	99.64	0.015	27.37	119.2	0.024	26.99	130	0.003	0.094	−0.325
CWMF 5×5 ($w = 9$)	16.65	1406	0.264	28.14	99.82	0.017	26.79	136.1	0.025	26.97	130.6	0.004	0.130	−0.469
CWMF 5×5 ($w = 11$)	18.06	1017	0.307	27.94	104.6	0.019	26.15	157.8	0.027	26.78	136.7	0.006	0.169	−0.487
Lee 5×5	25.16	198.2	0.443	28.13	100.1	0.021	27.23	123	0.024	27.24	122.7	0.006	0.423	1.112
Lee 7×7	25.09	201.4	0.439	27.87	106.3	0.020	26.57	143.2	0.023	27.23	123	0.005	0.487	1.049
DCT 7×7	25.14	199	0.471	29.68	69.99	0.017	29.48	73.34	0.023	28.74	86.9	0.003	0.486	0.806
DCT 8×8	25.14	199.3	0.471	29.76	68.70	0.018	29.48	73.26	0.023	28.9	83.7	0.003	0.488	0.729
DCT 9×9	25.16	198.2	0.471	29.68	69.95	0.017	29.65	70.50	0.023	28.99	82.1	0.003	0.389	0.444

corresponds to a locally passive area to be processed by NSF, and if $\vartheta_{ij} > \vartheta_t$, it belongs to a locally active area to be filtered by DPF.

We now briefly consider the most typical LAIs. For multiplicative noise case they are the relative local variance (RLV) and the normalized quasirange (NQ) [20] derived as follows:

$$\sigma_{rij}^2 = \sum_{k=i-(N-1)/2}^{i+(N-1)/2} \sum_{l=j-(N-1)/2}^{j+(N-1)/2} \frac{(I_{kl} - \bar{I}_{ij})^2}{(m^2-1)\bar{I}_{ij}^2},$$
$$Q_{nij} = \frac{I_{ij}^{(p)} - I_{ij}^{(q)}}{I_{ij}^{(p)} + I_{ij}^{(q)}}, \tag{5}$$

where $\bar{I}_{ij} = \sum_{k=i-(N-1)/2}^{i+(N-1)/2} \sum_{l=j-(N-1)/2}^{j+(N-1)/2} I_{kl}/m^2$ is the local mean, $N = m \times m$ denotes the scanning window size, $I_{ij}^{(p)}$ and $I_{ij}^{(q)}$ are the pth- and qth-order statistics determined for the ijth scanning window position, $p+q = N+1$. In our experiments we used $p \approx 0.76N$ and $q \approx 0.24N$.

Numerical simulation results for two versions of the two-state LAF (based on RLV and NQ used as ϑ_{ij} in (4)) are presented in Table 2 (two-state switching scheme). The two component filters (NSF and DPF) were the 7×7 L_{pq}-filter [20, 23] (for which the output was calculated as $I_{ij}^{L_{pq}} = (I_{ij}^{(p)} + I_{ij}^{(q)})/2$, $p \approx 0.8N$ and $q \approx 0.2N$, $p+q = N+1$) and the 7×7 MSF [18].

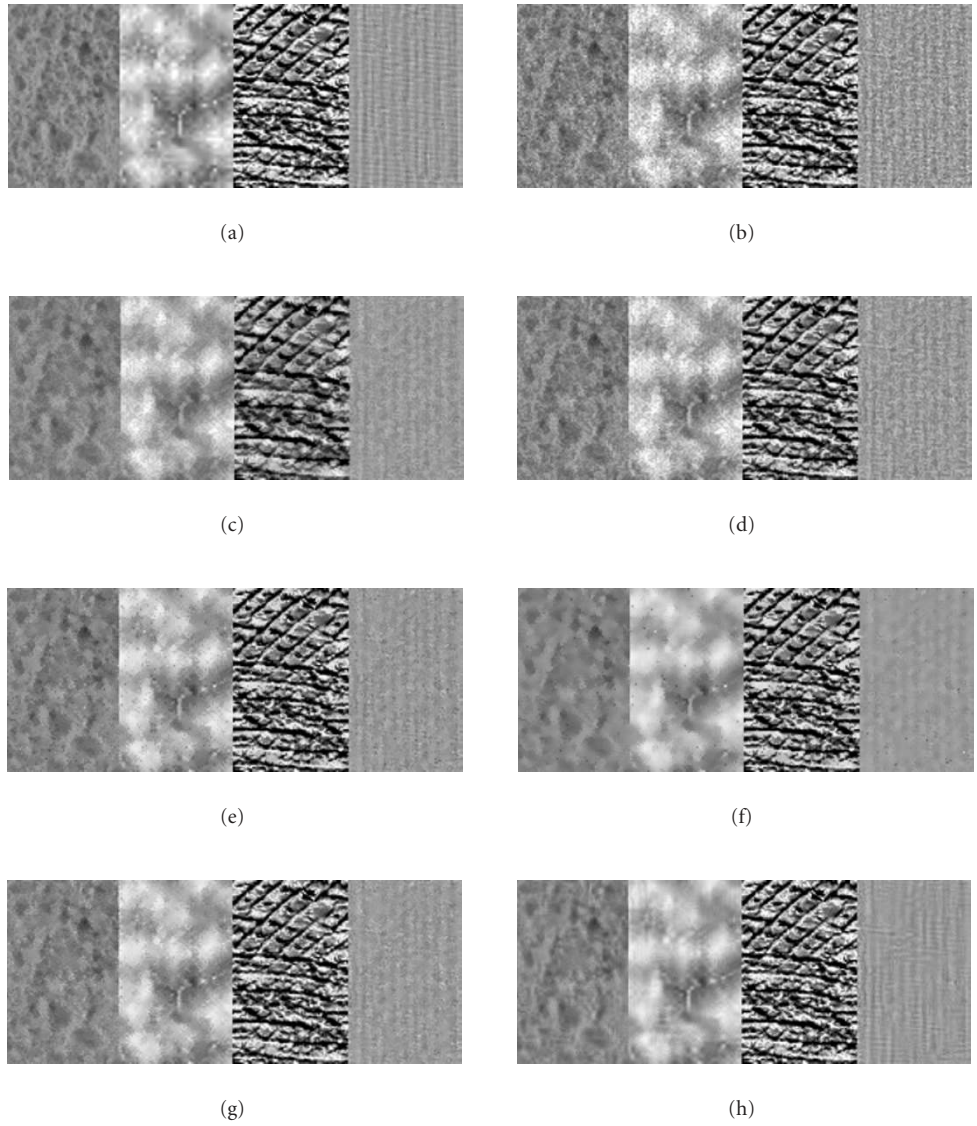

(a) (b) (c) (d) (e) (f) (g) (h)

FIGURE 6: Visual representation of filtering results of four texture samples corrupted by (a) multiplicative noise $\sigma_\mu^2 = 0.012$, and (b) by different DPFs: (c) the 5×5 CWMF with the central element weight 11, (d) the FMHF, (e) the 5×5 sigma filter, (f) the 5×5 MSF, (g) the 5×5 local statistic Lee filter, and (h) the 8×8 DCT-based filter.

As seen, the aggregate MSE and PSNR calculated for entire image are improved only a little in comparison to the 7×7 modified sigma filter. However, the improvement in image homogeneous regions due to application of the 7×7 L_{pq}-filter to them is of about 1 dB. The local MSE and PSNR in edge/detail and texture areas are practically the same as for the modified sigma filter since this filter is mostly used for processing the image in these areas.

The output of this two-state LAF applied to the noisy image in Figure 7a is presented in Figure 7b. Efficient noise suppression in HRs and good edge/detail preservation are observed. But the texture in texture regions (TRs) is distorted (compare the images in Figures 7b and 1).

We consider the possibilities to get around these shortcomings by developing three-state LAFs. In general, the three-state locally adaptive filter can be defined as

$$I_{ij}^{f} = \begin{cases} I_{ij}^{\mathrm{NSF}}, & S_{ij}^{3\,\mathrm{st}} = 1, \\ I_{ij}^{\mathrm{DPF}}, & S_{ij}^{3\,\mathrm{st}} = 2, \\ I_{ij}^{\mathrm{TPF}}, & S_{ij}^{3\,\mathrm{st}} = 3, \end{cases} \tag{6}$$

where now, opposite to (4), the PC ($S_{ij}^{3\,\mathrm{st}}$) can get three values—1, 2, and 3. The latter corresponds to the case of the given pixel classification as belonging to TR for which the texture preserving filter (TPF) is applied (its output is denoted as I_{ij}^{TPF}).

Recall that our task in three-state hard-switching LAF design is to detect and localize the regions with different types of texture. Therefore, only the features common for various

Table 2: Aggregate and local MSE and PSNR values for nonadaptive and locally adaptive filters for the test image in Figure 1 containing four texture fragments. The multiplicative Gaussian noise with $\sigma_\mu^2 = 0.005$ and with $\sigma_\mu^2 = 0.012$ has been added to this image (see Figure 7a).

The component filters for LAF ($\boldsymbol{\sigma_\mu^2} = 0.005$)\[$\boldsymbol{\sigma_\mu^2} = 0.012$]: HR—sum-rank filter 7×7 ($q = 12$, $p = 38$); TR—DCT-filter ($t_{\mathrm{DCT}} = 8$)\[$t_{\mathrm{DCT}} = 13$]; EDNR—MSF 7×7 ($\sigma_r^2 = 0.005$)\[$\sigma_r^2 = 0.012$]			Entire image		Homogeneous regions		Edge neighborhoods		Texture regions	
			PSNR	MSE	PSNR	MSE	PSNR	MSE	PSNR	MSE
Corrupted by multiplicative Gaussian noise with $\sigma_\mu^2 = 0.005$			29.23	77.56	30.05	64.22	29.32	76.02	27.2	123.88
Sum-rank filter 7×7			21.9	419.73	45.84	1.7	18.57	904.7	19.57	717.57
Sigma-filter 7×7 ($\sigma_r^2 = 0.005$)			33.9	26.5	37.72	10.99	34.36	23.85	28.98	82.18
Sigma-filter 7×7 ($\sigma_r^2 = 0.007$)			34.57	22.69	39.84	6.75	35.1	20.11	29.12	79.61
Sigma-filter 5×5 ($\sigma_r^2 = 0.005$)			33.72	27.62	36.94	13.16	34.02	25.8	29.2	78.16
Sigma-filter 5×5 ($\sigma_r^2 = 0.007$)			34.48	23.17	38.79	8.59	34.8	21.52	29.46	73.7
Modified sigma-filter 7×7 ($\sigma_r^2 = 0.005$)			34.83	21.37	44.16	2.5	35.58	18.01	28.62	89.43
Lee filter 7×7 ($\sigma_r^2 = 0.007$)			32.07	40.36	36.56	14.37	30.2	62.09	29.26	77.11
Lee filter 5×5 ($\sigma_r^2 = 0.008$)			32.82	33.96	37.18	12.46	31.12	50.25	29.81	67.99
DCT ($t_{\mathrm{DCT}} = 8$)			34.3	24.19	41.59	4.51	31.93	41.68	31.16	49.78
2-state switching scheme		RLV ($\vartheta_t = 0.0063$)	34.9	21.07	45.69	1.76	35.58	18.01	28.59	89.89
		NQ ($\vartheta_t = 0.07$)	34.84	21.33	44.36	2.38	35.57	18.03	28.61	89.51
3-state switching scheme	2-threshold	RLV ($\vartheta_{t1} = 0.0068$; $\vartheta_{t2} = 0.015$)	35.45	18.54	45.54	1.82	34.94	20.83	29.84	67.44
		NQ ($\vartheta_{t1} = 0.07$; $\vartheta_{t2} = 0.17$)	35.01	20.5	45.65	1.77	33.7	27.74	29.99	65.2
	Iterative	RLV ($\vartheta_{t1} = 0.006$; [$T_{\mathrm{TR}}(\%) = 74\%$; $M = 2.6m$])	35.55	18.14	44.77	2.17	33.91	26.41	31	51.69
		NQ ($\vartheta_{t1} = 0.11$; [$T_{\mathrm{TR}}(\%) = 61\%$; $M = 2.5m$])	36	16.32	45.16	1.98	34.84	21.33	31.01	51.66
	CPC1		36.45	14.74	45.37	1.89	35.95	16.51	30.95	52.27
	CPC2		36.37	15	45.78	1.72	36.02	16.25	30.72	55.11
Corrupted by multiplicative Gaussian noise with $\sigma_\mu^2 = 0.012$			25.62	178.39	26.43	147.97	25.69	175.46	23.62	282.74
Sum-rank filter 7×7			22.05	405.27	42.17	3.94	18.8	857.18	19.55	720.8
Sigma-filter 7×7 ($\sigma_r^2 = 0.012$)			30.71	55.22	33.75	27.42	30.7	55.35	26.53	144.54
Sigma-filter 7×7 ($\sigma_r^2 = 0.022$)			31.81	42.88	37.21	12.36	31.6	45.03	26.78	136.56
Sigma-filter 5×5 ($\sigma_r^2 = 0.012$)			30.52	57.72	33.04	32.27	30.51	57.87	26.69	139.4
Sigma-filter 5×5 ($\sigma_r^2 = 0.025$)			31.93	41.7	36.6	14.23	31.7	44.01	27.16	125.2
Modified sigma-filter 7×7 ($\sigma_r^2 = 0.012$)			32.26	38.64	40.51	5.79	32.16	39.58	26.6	142.43
Lee filter 7×7 ($\sigma_r^2 = 0.017$)			29.96	65.7	37.55	11.44	27.32	120.65	27.28	121.65
Lee filter 5×5 ($\sigma_r^2 = 0.018$)			30.66	55.9	36.98	13.04	28.33	95.62	27.79	108.06
DCT ($t_{\mathrm{DCT}} = 13$)			31.4	47.08	39.31	7.63	28.71	87.57	28.76	86.58
2-state switching scheme		RLV ($\vartheta_t = 0.015$)	32.3	38.32	41.34	4.78	32.16	39.55	26.56	143.73
		NQ ($\vartheta_t = 0.12$)	32.29	38.41	41.02	5.14	32.16	39.57	26.58	143.09
3-state switching scheme	2-threshold	RLV ($\vartheta_{t1} = 0.014$; $\vartheta_{t2} = 0.036$)	32.77	34.37	41.14	5.01	31.7	43.92	27.78	108.32
		NQ ($\vartheta_{t1} = 0.12$; $\vartheta_{t2} = 0.3$)	32.67	35.14	40.49	5.81	31.37	47.4	28	103.16
	Iterative	RLV ($\vartheta_{t1} = 0.014$; [$T_{\mathrm{TR}}(\%) = 77\%$; $M = 2.6m$])	32.5	36.57	40.59	5.67	30.53	57.54	28.55	90.76
		NQ ($\vartheta_{t1} = 0.135$; [$T_{\mathrm{TR}}(\%) = 69\%$; $M = 2.6m$])	32.81	34.05	41.29	4.84	31.4	47.13	28.14	99.85
	CPC1		32.9	33.36	41.42	4.69	31.29	48.33	28.43	93.31
	CPC2		33.44	29.47	41.92	4.18	32.72	34.74	28.15	99.54

texture types can be exploited. Such features can be verbally described as follows. Texture is mostly *slight (not very intensive) spatial variations* of the image true values *in the regions of the size not less than ten to ten pixels* (although the first assumption is not absolutely true for intensive texture like for the first, upper-left texture fragment of the test image). Therefore, the texture detectors should be suited (sensitive) for such kind of variations. Taking into account that noise

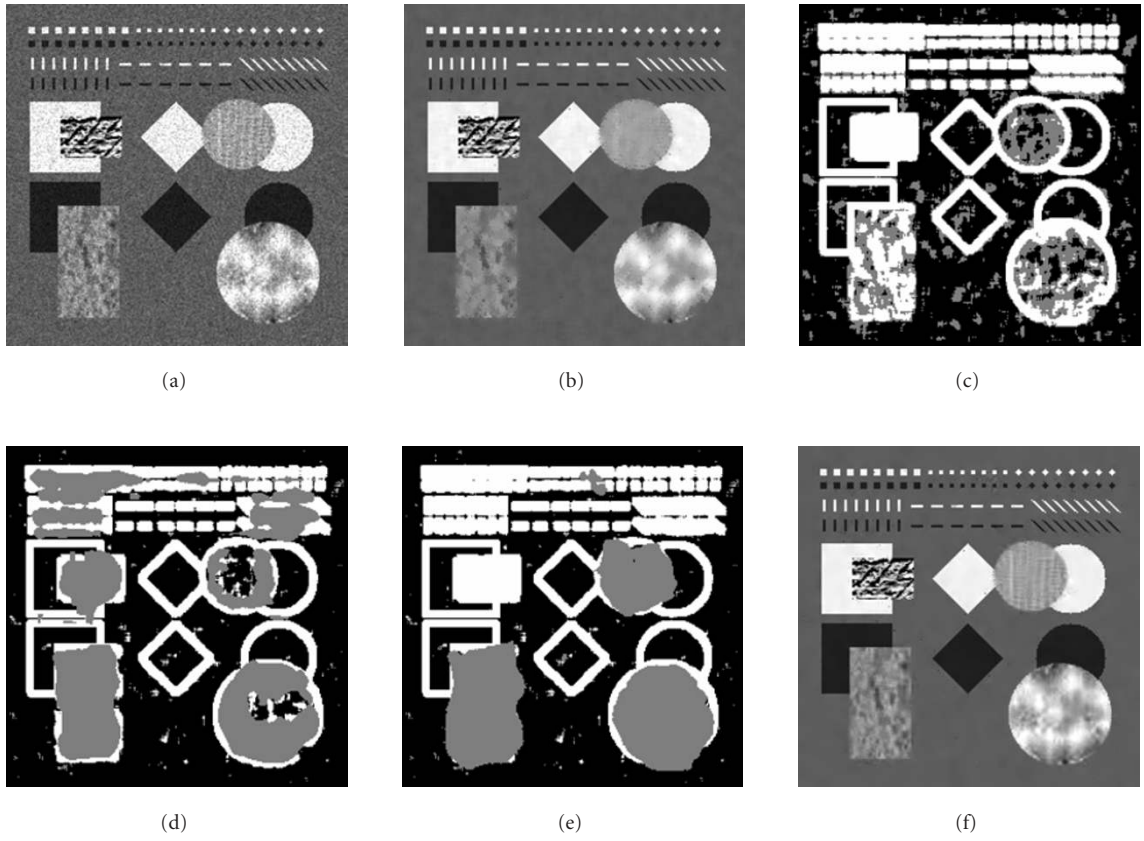

(a) (b) (c)

(d) (e) (f)

Figure 7: Examples of the test image (Figure 1) processing: (a) the test image corrupted by multiplicative Gaussian noise with $\sigma_\mu^2 = 0.012$, (b) the output of the two-state hard-switching LAF, (c) the result of two-threshold preclassification (7), (d) the "CPC1" classification map, (e) the "CPC2" classification map, and (f) the output of the three-state hard-switching LAF processing according to the CPC2 map.

is present in images, we can also give quantitative definition of texture—for images corrupted by multiplicative noise in texture regions, σ^2 should be comparable or larger than σ_μ^2.

One simple idea [14] is to apply for calculation of $S_{ij}^{3\,\mathrm{st}} = S_{ij}^{2\,\mathrm{thr}}$ the two-threshold scheme like

$$\begin{aligned} S_{ij}^{2\,\mathrm{thr}} &= 1 \quad \text{if } \vartheta_{ij} \le \vartheta_{t1}, \\ S_{ij}^{2\,\mathrm{thr}} &= 2 \quad \text{if } \vartheta_{t1} < \vartheta_{ij} \le \vartheta_{t2}, \\ S_{ij}^{2\,\mathrm{thr}} &= 3 \quad \text{if } \vartheta_{ij} > \vartheta_{t2}, \end{aligned} \tag{7}$$

where ϑ_{t1} and ϑ_{t2} are the thresholds.

However, the results of such preclassification application are not appropriate [14] since the texture has not been detected well enough. As seen in Figure 7c, more than half of the left-bottom texture region is classified as edge/detail areas and intensive texture region (left-top) is fully classified as edge/detail areas; in this map grey color shows detected TRs, black color corresponds to the pixels classified as HR, white ones relate to EDNRs. Other texture regions are also classified not correctly enough. The reason is the empiric selection of the thresholds ϑ_{t1} and ϑ_{t2}. They are set as $\vartheta_{t1} \approx 1.3\sigma_\mu^2$ and $\vartheta_{t2} \approx 3\sigma_\mu^2$ for the RLV (5) used as LAI, and $\vartheta_{t1} \approx 0.05 + 0.6\sigma_\mu$ and $\vartheta_{t2} \approx 0.05 + 2\sigma_\mu$ for the NQ (5). The drawbacks of this approach to texture detection also deal with the fact that it in no way takes into account the property of texture to occupy rather large spatial areas.

However, even for this, not perfect three-state LAF the aggregate and the local texture MSE and PSNR have improved in comparison to the two-state LAF (see the corresponding data in Table 2). The basic reason for this is that DCT-based filter has been applied, at least, to some fragments of texture regions.

Another proposed method for TR detection and localization implies using spatial properties of texture, that is, its property to "cover" some space. For more complicated and efficient PCs with three states $S_{ij}^{3\,\mathrm{st}}$ we have proposed [14] to apply the iterative approach for which the PC map is formed as

$$S_{ij}^{3\,\mathrm{st}} = \begin{cases} S_{ij}^{2t(\mathrm{LAI})}, & \xi_{ij}^{\mathrm{H}} \le T_{\mathrm{TR}}(\%), \\ 3, & \xi_{ij}^{H} > T_{\mathrm{TR}}(\%), \end{cases} \tag{8}$$

$$\text{where } \xi_{ij}^{H} = \xi_{ij}^{1t(\mathrm{LAI})} = \left[\sum_{k,l=-(M-1)/2}^{(M-1)/2} \frac{S_{i+k,j+l}^{1t(\mathrm{LAI})} - 1}{M^2} \right] \cdot 100\%,$$

where $\xi_{ij}^{2t(\mathrm{LAI})}$ is the two-threshold LAI value (calculated using (5) and (7)), ξ_{ij}^{H} is the heterogeneity indicator expressed in percent for $M \times M$ window. The value of M in the iterative procedure (8) should be approximately 2.5 times larger than the scanning window side size m for the initial stage of LAI calculation (5) for which m was set equal to 7. $T_{\mathrm{TR}}(\%)$ is the threshold value of heterogeneity percentage indicator. As ξ_{ij}^{H} in case of iterative approach, the one-threshold $\xi_{ij}^{1t(\mathrm{LAI})}$ was used. It is calculated using one-threshold LAI $S_{ij}^{1t(\mathrm{LAI})}$ ($S_{ij}^{1t(\mathrm{LAI})} = 1$ if $Q_{ij} > \vartheta$ and $S_{ij}^{1t(\mathrm{LAI})} = 0$ if $Q_{ij} \le \vartheta$) in $M \times M$ window. As LAI in (8), the same LAI was used, either RLV or NQ. The optimal threshold $T_{\mathrm{TR}}(\%)$ was about 60–80%. This simple approach was tested earlier in [14].

The numerical simulation results for this approach are presented in Table 2 and marked as "iterative." Due to better preclassification of TRs, the three-state LAF performance has been again improved in comparison to the two-threshold three-state hard-switching LAF. Texture preservation has become almost the same as for the DCT-based filter.

A little bit more complex and efficient approach to forming the PC with three states $S_{ij}^{3\,\mathrm{st}}$ for more accurate TR detection and localization proposed [15] is to apply the combined iterative approach where the PC map $\{S_{ij}^{\mathrm{Cmb}}\}$ is formed as

$$S_{ij}^{3\,\mathrm{st}} = S_{ij}^{\mathrm{Cmb}} = \begin{cases} S_{ij}^{2t(\mathrm{RLV})}, & \xi_{ij}^{H} \le T_{\mathrm{TR}}(\%), \\ 3, & \xi_{ij}^{H} > T_{\mathrm{TR}}(\%), \end{cases} \tag{9}$$

$$\text{where } \xi_{ij}^{H} = \xi_{ij}^{1t(\mathrm{NQ})} = \left[\sum_{k,l=-(M-1)/2}^{(M-1)/2} \frac{S_{i+k,j+l}^{1t(\mathrm{NQ})} - 1}{M^2} \right] \cdot 100\%.$$

As can be seen the fixed scheme of combined exploiting the $S_{ij}^{2t(\mathrm{RLV})}$ (calculated using (5) and (7)) and $S_{ij}^{1t(\mathrm{NQ})}$ (see (7)) is used in this case. Recall that in this case $\xi_{ij}^{1t(\mathrm{NQ})}$ is calculated for only one threshold ($S_{ij}^{1t(\mathrm{NQ})} = 1$ if $Q_{ij} > \vartheta$ and $S_{ij}^{1t(\mathrm{NQ})} = 0$ if $Q_{ij} \le \vartheta$). So this PC has got the name of combined PC 1 (CPC1). The recommendation concerning M and $T_{\mathrm{TR}}(\%)$ values are the same as for iterative procedure (8).

Numerical simulation results for this approach (see Table 2) marked as "CPC1" show noticeable improvement of edge neighborhoods region filtering. However, the misclassifications are observed in the areas of many small-sized objects concentration (Figure 7d) and this is the drawback of this preclassification method. This drawback deals with the fact that it is very difficult to discriminate the areas of detail concentration and texture fragments.

To get rid of these drawbacks the combined PC 2 (CPC2) was proposed. This approach assumes using the $\xi_{ij}^{2t(\mathrm{NQ})}$ as heterogeneity indicator ξ_{ij}^{H} instead of $\xi_{ij}^{1t(\mathrm{NQ})}$ used by CPC1. For CPC2 the parameter $\xi_{ij}^{2t(\mathrm{NQ})}$ is calculated based on two-threshold LAI $S_{ij}^{2t(\mathrm{NQ})}$ as follows:

$$\xi_{ij}^{2t(\mathrm{NQ})} = \left[\sum_{k,l=-(M-1)/2}^{(M-1)/2} \frac{\chi_{ij}}{M^2} \right] \cdot 100\%,$$
$$\text{where } \chi_{ij} = \begin{cases} 1, & S_{ij}^{2t(\mathrm{NQ})} = 3, \\ 0, & S_{ij}^{2t(\mathrm{NQ})} = 1 \text{ or } 2. \end{cases} \tag{10}$$

The CPC2 permits to avoid misclassifications in places of small detail concentration. CPC2 also better than CPC1 localizes low-contrast textures (compare the classification maps in Figures 7d and 7e). The only drawback of CPC2 is misclassification of very high-contrast texture (left-top) as edge/detail region. Because of noticeable loss of PSNR in this region (actually, the local PSNR for the left-top texture processing for CPC1 is 29.03 compared to 26.98 for CPC2), the three-state LAF based on CPC2 is characterized by 0.08 dB worse PSNR for entire image than the three-state LAF based on CPC1 (for $\sigma_{\mu}^2 = 0.005$). Nevertheless, since such characteristics as very high contrasts are not very typical for textures, we can consider the CPC2 classification as conceptually more correct. Moreover, even despite aforementioned misclassifications, the three-state LAF based on CPC2 ensures noticeable PNSR increasing compared to that one based on CPC1 in the case of larger multiplicative noise variance (see data in Table 2 for $\sigma_{\mu}^2 = 0.012$).

For CPC2 we recommend to use the following thresholds: for RLV set $\vartheta_{t1} \approx 1.3\sigma_{\mu}^2$, $\vartheta_{t2} \approx 1.9\sigma_{\mu}^2$; for NQ use $\vartheta_{t1} \approx 0.05 + 0.9\sigma_{\mu}$, $\vartheta_{t2} \approx 0.05 + 2.5\sigma_{\mu}$. The value M in (9), (10) for CPC2 should be approximately 3 times larger than m; the optimal threshold $T_{\mathrm{TR}}(\%)$ is about 45–55%.

Despite of aforementioned misclassification, the quantitative results for the three-state LAFs based on combined preclassification procedures are either the best or very close to the best reachable according to the aggregate and all local MSE and PSNR criteria (see Table 2). The main advantage of combined PCs is that the basic objective, that is, good preservation of texture features, has been attained simultaneously with effective noise reduction in image HRs and appropriate edge/detail preservation. This fact is illustrated in Figure 8 where visual processing results comparison for three-component LAF with CPC2 and its component filters are presented. As can be seen, each of component filters possesses its own advantages: the L_{pq}-filter produces the highest noise suppression in homogeneous regions (Figure 8b), the MSF ensures very good noise suppression with detail preservation in edge/detail regions (Figure 8c), the DCT filter provides good noise suppression with detail preservation in texture region (Figure 8d). At the same time these images shows the drawbacks of component filters. The proposed three-state LAF with CPC2 provides the opportunity to combine efficiently the component filter advantages and eliminate their drawbacks (Figure 8e).

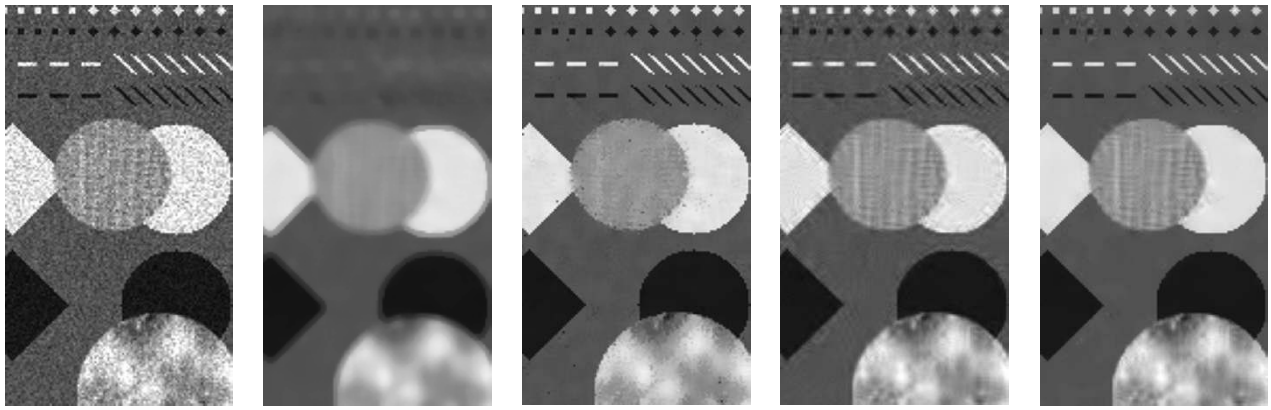

(a) (b) (c) (d) (e)

Figure 8: The visual results of processing the test image (Figure 1) fragment by component filters and their final nonlinear composition: (a) the test image fragment corrupted by multiplicative Gaussian noise with $\sigma_\mu^2 = 0.012$, (b) the output of 7×7 L_{pq} filter, (c) the output of 7×7 MSF filter, (d) the output of 8×8 DCT filter, and (e) the output of the three-state hard-switching LAF.

The full-output test image for the three-state LAF based on CPC2 is presented in Figure 7f. Obviously, the considerably better texture preservation is ensured compared to the image in Figure 7b.

5. THREE-STATE LOCALLY ADAPTIVE FILTER FOR ADDITIVE NOISE CASE

We now consider the simulation results obtained for dominant influence of additive noise (image model (2)). Two variance values $\sigma_n^2 = 100$ and $\sigma_n^2 = 200$ have been considered. For additive noise case, as LAIs we used the local variance and quasirange defined as

$$\sigma_{lij}^2 = \sum_{k=i-(N-1)/2}^{i+(N-1)/2} \sum_{l=j-(N-1)/2}^{j+(N-1)/2} \frac{(I_{kl} - \bar{I}_{ij})^2}{m^2 - 1}, \qquad (11)$$

$$Q_{lij} = I_{ij}^{(p)} - I_{ij}^{(q)},$$

where $N = m \times m = 7 \times 7$ and, as in previous experiments, $p \approx 0.76N$ and $q \approx 0.24N$.

A more narrow set of component filters has been studied, namely the L_{pq} noise suppressing filter, the standard sigma filter and the MSF for additive noise [36], and the DCT-based filter version for additive noise [38]. Exact values of additive noise variance have been used as input parameters of the standard and modified sigma filters.

As earlier, the L_{pq}-NSF and the MSF [36] have been used as components of two-state hard-switching LAF, the thresholds have been set according to recommendations given in [20]. The same filters plus the DCT-based filter have been in the staff of three-state LAF. Besides, below we consider only one, the best, version of preclassifier, namely, the CPC2. The recommended values of the thresholds for additive noise case are the following: for local variance (11) set $\vartheta_{t1} \approx 1.7\sigma_n^2$, $\vartheta_{t2} \approx 1.9\sigma_n^2$; and for quasirange (11) apply $\vartheta_{t1} \approx 2.4\sigma_n$, $\vartheta_{t2} \approx 4.5\sigma_n$. Other settings of the preclassification algorithm parameters are $M \approx 3m$; $T_{\mathrm{TR}}(\%)$ is about 45–55%.

The obtained simulation data for the test image in Figure 1 corrupted by additive noise are presented in Table 3. Its analysis shows that the basic tendencies and dependencies earlier observed for multiplicative noise case (see Section 4) are the same. Again, the 7×7 L_{pq}-NSF is the best for HR processing while the 7×7 MSF preserves edges and details in the best manner. The DCT-based filtering produces the most efficient processing of TRs although the benefit due to its application depends upon the texture type.

In turn, the proposed three-state LAF provides the maximal PSNR for entire image as well as the local PSNRs that are the best or, at least, approach to the best reachable values. Clearly, the three-state LAF outperforms the two-state one, and the basic difference in their performance is observed for texture regions. As the result, the difference of about 1 dB is observed for PSNRs evaluated for entire image.

The test image fragment corrupted by additive noise with $\sigma_n^2 = 200$ is presented in Figure 9a. If DCT-based filtering is applied to entire image, one obtains the image represented in Figure 9b. Similarly to multiplicative noise case (see Figure 8), the basic drawback of the DCT-based filter is observed in the neighborhoods of high-contrast edges and small-sized objects where ringing artifacts are rather clearly seen. Besides, residual fluctuations are visible in image homogeneous regions. These shortcomings are got around in the case of the three-state LAF application (see Figure 9c).

In addition, the simulations for the typical optical test image "Barbara" corrupted by Gaussian additive noise with $\sigma_n^2 = 100$ have been performed and presented in fragmentary form in Figure 10. The noisy image is represented in Figure 10a and the proposed three-state LAF output (Figure 10c) can be compared to the two-state LAF output (Figure 10b). As can be seen, the texture-related areas (e.g., those that belong to face and chair back areas) are processed by the three-state LAF with higher quality (Figure 10c)

Table 3: Aggregate and local PSNR values for nonadaptive and locally adaptive filters for the test image in Figure 1. The additive Gaussian noise with $\sigma_n^2 = 100$ and with $\sigma_n^2 = 200$ has been added to this image (Figure 8a).

The component filters for LAF ($\sigma_n = 100$)\[$\sigma_n = 200$]: HR—sum-rank filter; TR—DCT-filter; EDN—MSF 7×7 ($\sigma_n^2 = 100$)\[$\sigma_n^2 = 200$]		PSNR							
		Entire image	HRs	EDNRs	TRs (in aggregate)	Separately for different texture regions			
						Cement	Bread	Linen	Cracks
Corrupted with $\sigma_n^2 = 100$		28.15	28.15	28.12	28.23	28.76	28.19	28.25	28.13
Sum-rank filter 5×5 ($q = 8$, $p = 18$)		23.63	41.03	20.56	20.73	11.77	26.87	26.36	28.35
Sum-rank filter 7×7 ($q = 12$, $p = 38$)		21.97	43.83	18.67	19.58	10.68	25.31	25.81	26.61
Sigma-filter 5×5		33.30	35.45	33.23	29.83	27.97	29.90	30.05	30.3
Sigma-filter 7×7		33.59	36.29	33.54	29.66	28.14	29.72	30.11	29.89
Modified sigma-filter 5×5		34.5	40.9	34.5	29.08	25.95	29.37	28.97	30.22
Modified sigma-filter 7×7		34.72	43	34.64	29.04	26.61	29.18	29.18	29.75
DCT 8×8 ($t_{\mathrm{DCT}} = 20$)		33.2	37.08	31.05	31.37	28.86	31.14	31.41	32.56
2-state switching scheme	RLV	34.76	43.86	34.65	29	26.61	29.13	29.09	29.73
	NQ	33.04	43.87	31.03	28.75	26.61	28.82	28.41	29.64
3-state switching scheme based on CPC2		35.9	43.86	35.02	30.83	26.61	31.12	31.41	32.45
Corrupted with $\sigma_n^2 = 200$		25.15	25.14	25.15	25.15	25.81	25.01	25.01	25.25
Sum-rank filter 5×5 ($q = 8$, $p = 18$)		23.57	38.13	20.57	20.66	11.73	26.72	26.12	28.09
Sum-rank filter 7×7 ($q = 12$, $p = 38$)		22.02	40.92	18.77	19.53	10.64	25.27	25.67	26.49
Sigma-filter 5×5		30.44	32.26	30	27.73	25.18	27.76	28.11	28.5
Sigma-filter 7×7		30.68	33.08	30.09	27.56	25.32	27.58	28.28	28.02
Modified sigma-filter 5×5		32.09	37.75	31.24	27.5	23.38	27.88	27.88	29.04
Modified sigma-filter 7×7		32.17	40.04	31.1	27.27	24.03	27.48	27.94	28.14
Fast DCT 8×8 ($t_{\mathrm{DCT}} = 28$)		30.83	34.39	28.73	29.19	26.12	29.07	29.42	30.51
2-state switching scheme	RLV	32.21	40.67	31.11	27.23	24.03	27.42	27.86	28.11
	NQ	31.01	40.88	29.03	26.78	24.03	26.74	27.07	27.78
3-state switching scheme based on CPC2		32.86	40.74	31.2	28.57	24.03	28.95	29.19	30.38

compared to its two-component predecessor (Figure 10b). The PSNR results show 2.4 dB improvement provided by the two-state LAF and 5.3 dB improvement ensured by the three-state hard-switching LAF. As can also be seen, the residual noise and distortions are practically not seen in the image in Figure 10c.

6. EXAMPLES OF THREE-STATE LAF APPLICATION TO REAL RS IMAGES

The methods of image preclassification and processing based on three-state locally adaptive filtering have been also studied using real-life SLAR and SAR images. An example of K_a-band SLAR image is presented in Figure 11. It has been obtained by airborne radar designed and exploited by the Center of Radiophysical Earth Sensing, Ukrainian National Academy of Science and National Space Agency, Kharkov, Ukraine. For this image, the estimated multiplicative noise variance was 0.005, that is, just like in simulations presented in Section 4.

Comparing the image in Figure 11a to the preclassification map in Figure 11b, it is seen that the image fragments that either contain obvious texture or do not have very intensive local variations of radar cross section are reliably referred to TRs. At the same time, small-sized and prolonged objects that commonly appear as lighter pixels than the surrounding background or are considerably darker like the river in the lower part of the image are also reliably identified as edge/detail neighborhoods and preserved well (see Figure 11c).

The X-band SLAR image formed by aforementioned airborne multichannel radar complex is shown in Figure 12a. The estimated multiplicative noise variance for this image was 0.012, that is, the same as we used in our simulation experiments (see Section 4). The modified sigma filter output is represented in Figure 12b. Although the noise in HRs is suppressed and the edges and details are preserved well enough, the texture looks smeared and distorted. The three-state LAF has been applied to the original image using CPC2 (Figure 12c), its output is given in Figure 12c. As seen, the texture is preserved better in comparison to MSF while noise suppression and edge-detail preservation are also attained.

Besides, we would like to demonstrate that the proposed three-state LAF can be, with the corresponding preprocessing, applied to SAR image processing. In [37, 41] it has been proven that both MSF and DCT-based denoising can be successfully applied sequentially to the local statistic Lee output in the case the original pdf of speckle is essentially non-Gaussian. The application of the Lee filter at initial stage

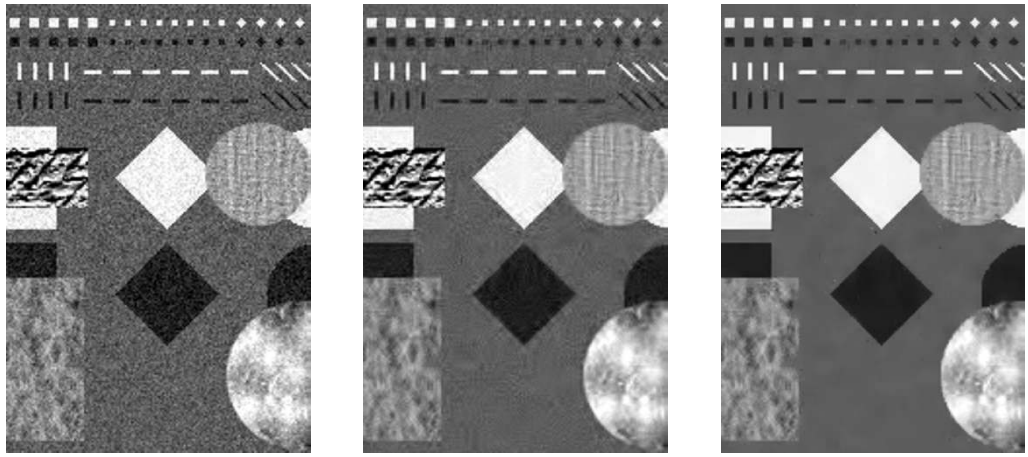

(a) (b) (c)

Figure 9: Visual results of processing the test image corrupted by Gaussian noise with $\sigma_n^2 = 200$: (a) original noisy image, (b) the 8×8 DCT filter output, and (c) the result of image processing by the proposed three-component hard-switching LAF.

(a) (b) (c)

Figure 10: Visual results for processing the test image "Barbara" corrupted by (a) Gaussian noise with $\sigma_n^2 = 100$ (PSNR = 28.12 dB), (b) by the two-state hard-switching LAF (PSNR = 30.58 dB), and (c) by the proposed three-component hard-switching LAF (PSNR = 33.43 dB).

results in residual speckle normalization and this is put behind the idea to further use the filtering techniques suited to Gaussian noise pdf.

An airborne L-band SAR image with $\sigma_\mu^2 \approx 0.15$ is represented in Figure 13a. Obviously, it is severely degraded by speckle. All the output images (Figures 13b, 13c, and 13d) are obtained by means of filtering procedures that presume the aforementioned speckle normalizing preprocessing stage. The final output images after filtering by the 7×7 MSF and the two-state LAF are depicted in Figures 13b and 13c, respectively. As can be seen, speckle is considerably reduced but detail and texture information in most cases is lost. The output of the two-state LAF (Figure 13c) is also very similar to MSF output due to preprocessing phase and using MSF as component filter in LAF. The only difference between the MSF and two-state LAF outputs is that in latter case more details are lost due to misclassifying of small contrast details to homogeneous regions. At the same time, in Figure 13d one can see that the use of the proposed three-state LAF allows us to resolve the task of noise suppression and simultaneous information preservation in a rather good manner even in so complex noise situation.

7. CONCLUSIONS

The necessity to preserve texture features in images to be filtered has been underlined. Texture preserving properties of a wide set of filters have been thoroughly studied, higher-order statistics and 2D spatial correlation functions have been analyzed, and traditional criteria like MSE and PSNR

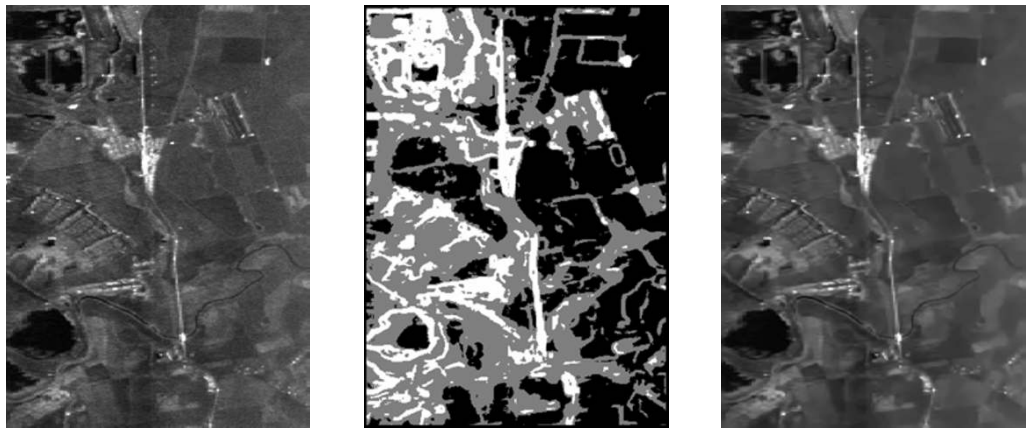

(a) (b) (c)

Figure 11: Visual example of the K_a-band SLAR image processing ($\sigma_\mu^2 \approx 0.005$): (a) the original image, (b) the PC map obtained by CPC2, and (c) the output of the proposed three-state LAF.

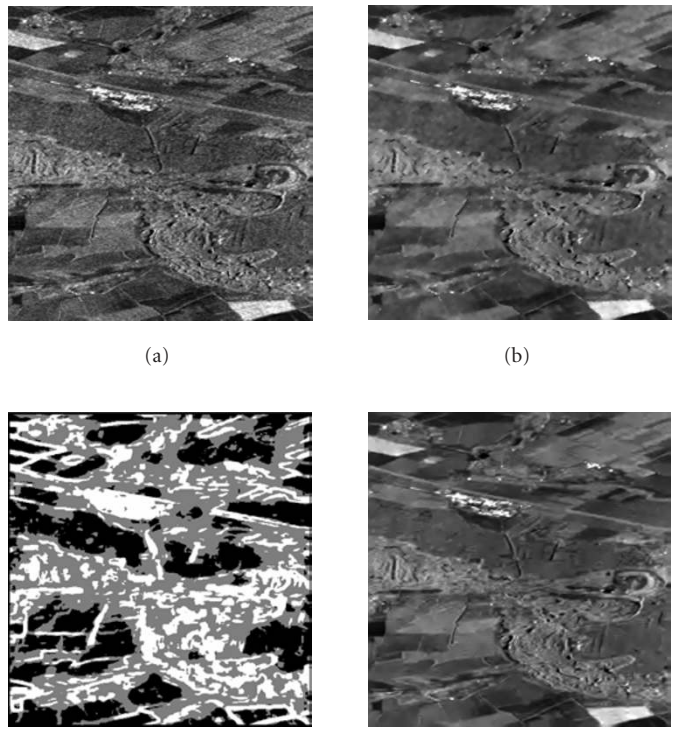

(a) (b)

(c) (d)

Figure 12: Visual example of SLAR image processing: (a) the original image, (b) the output of 7×7 MSF, (c) the PC map obtained by CPC2, and (d) the output of the proposed three-state LAF.

have been also taken into account. The study has been performed for four textures that considerably differed from each other. As for the result, we have shown that some filters that can be characterized as noise suppressing severely degrade texture. Among the filters that belong to detail preserving class the DCT-based filter has been found the best.

Several approaches to texture detection and localization have been considered and compared to each other. They have demonstrated rather good performance. Due to providing reliable texture detection, it has become possible to design the three-state locally adaptive hard switching filters that outperform known nonadaptive and locally adaptive filters.

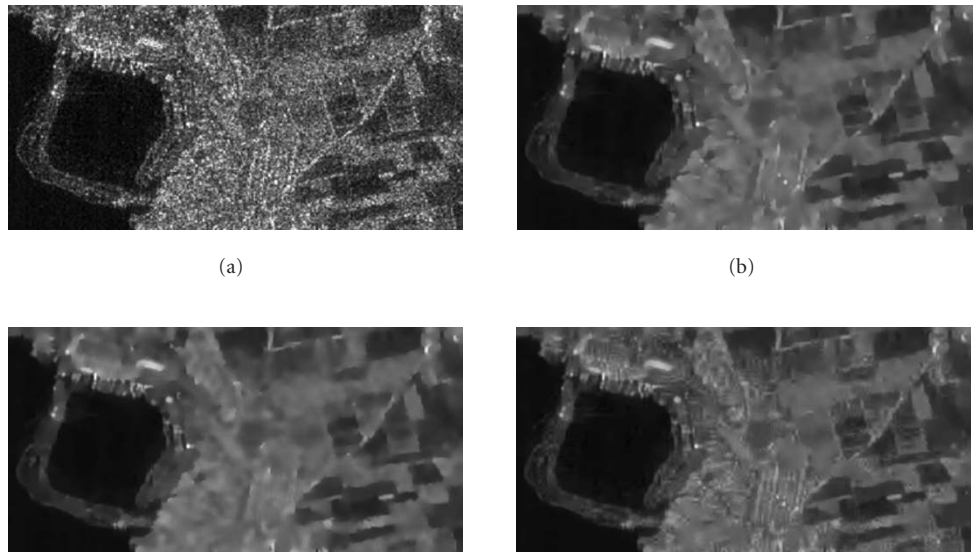

(a) (b)

(c) (d)

Figure 13: Real SAR image processing example: (a) the original L-band SAR image, (b) the output of MSF 7×7, (c) the output of two-component hard-switching LAF, and (d) the output of three-component hard-switching LAF. All filtering is performed implying preprocessing stage (see Section 6) for speckle normalization.

The reached PSNR improvement is about or more than 1–3 dB. This benefit is gained due to better texture preservation.

The applicability of the three-state LAFs is demonstrated for the real-life SLAR and SAR images. One optical grey scale image processing example is also given.

ACKNOWLEDGMENT

This work has been partly supported by the STCU Grant 1659.

REFERENCES

[1] R. M. Haralick, K. Shanmugam, and I. Dinstein, "Textural features for image classification," *IEEE Trans. Syst., Man, Cybern.*, vol. 3, no. 6, pp. 610–621, 1973.

[2] M. Datcu, D. Luca, and K. Seidel, "Multiresolution analysis of SAR images," in *Proc. European Conference on Synthetic Aperture Radar (EUSAR '96)*, pp. 375–378, Konigswinter, Germany, March 1996.

[3] H. Singh and A. Mahalanobis, "Correlation filters for texture recognition and applications to terrain-delimitation in wide-area surveillance," in *Proc. IEEE Int. Conf. Acoustics, Speech, Signal Processing (ICASSP '94)*, vol. 5, pp. V/153–V/156, Adelaide, SA, Australia, April 1994.

[4] D. Blacknell and R. G. White, "A comparison of neural network and classical texture analysis," in *IEE Seminar on Texture Analysis in Radar and Sonar*, pp. 5/1–5/7, London, UK, November 1993.

[5] A. P. Blake, D. Blacknell, and C. J. Oliver, "Texture simulation and analysis in coherent imagery," in *Proc. 5th International Conference on Image Processing and Its Applications*, pp. 772–776, Edinburgh, UK, July 1995.

[6] M. Partio, E. Guldogan, O. Guldogan, and M. Gabbouj, "Applying texture and color features to natural image retrieval," in *Proc. Finnish Signal Processing Symposium (FINSIG '03)*, pp. 199–203, Tampere, Finland, May 2003.

[7] J. C. Devaux, P. Gouton, and F. Truchetet, "Application of the Karhunen-Loeve transform to aerial color image segmentation," in *Proc. 4th International Conference on Knowledge-Based Intelligent Engineering Systems and Allied Technologies*, vol. 1, pp. 373–376, Brighton, UK, August–September 2000.

[8] J. Astola and P. Kuosmanen, *Fundamentals of Nonlinear Digital Filtering*, CRC Press, Boca Raton, Fla, USA, 1997.

[9] J. Xiuping and J. A. Richards, Eds., *Remote Sensing Digital Image Analysis: An Introduction*, Springer, Berlin, Germany, 3rd edition, 1999.

[10] D. Yunhan, A. K. Milne, and B. C. Forster, "A review of SAR speckle filters: texture restoration and preservation," in *Proc. IEEE International Geoscience and Remote Sensing Symposium (IGARSS '00)*, vol. 2, pp. 633–635, Honolulu, Hawaii, USA, July 2000.

[11] V. V. Lukin, J. T. Astola, V. P. Melnik, et al., "Data fusion and processing for airborne multichannel system of radar remote sensing: methodology, stages, and algorithms," in *Sensor Fusion: Architectures, Algorithms, and Applications IV*, vol. 4051 of *SPIE Proceedings*, pp. 215–226, Orlando, Fla, USA, April 2000.

[12] B. Aiazzi, L. Alparone, S. Baronti, and R. Carla, "Adaptive texture-preserving filtering of multitemporal ERS-1 SAR images," in *Proc. IEEE International Geoscience and Remote Sensing Symposium (IGARSS '97)*, vol. 4, pp. 2066–2068, Singapore, August 1997.

[13] S. W. Perry, H.-S. Wong, and L. Guan, *Adaptive Image Processing: A Computational Intelligence Perspective*, CRC Press, Boca Raton, Fla, USA, 2002.

[14] V. Lukin and O. Tsymbal, "MM-band radar image filtering with texture information preservation," in *Proc. 4th International Kharkov Symposium on Physics and Engineering of Millimeter and Sub-Millimeter Waves*, vol. 1, pp. 435–437, Kharkov, Ukraine, June 2001.

[15] V. V. Lukin, O. V. Tsymbal, N. N. Ponomarenko, K. O. Egiazarian, and J. T. Astola, "Image processing with texture feature preservation by three-state locally adaptive filter," in *Image and Signal Processing for Remote Sensing IX*, L. Bruzzone, Ed., vol. 5238 of *SPIE Proceedings*, pp. 120–131, Barcelona, Spain, September 2003.

[16] J.-S. Lee, "Speckle analysis and smoothing of synthetic aperture radar images," *Computer Graphics and Image Processing*, vol. 17, pp. 24–32, 1981.

[17] J.-S. Lee, "Digital image smoothing and the sigma filter," *Computer Vision, Graphics, and Image Processing*, vol. 24, no. 2, pp. 255–269, 1983.

[18] V. V. Lukin, N. N. Ponomarenko, A. A. Zelensky, P. Kuosmanen, and J. T. Astola, "Modified sigma filter for processing of images corrupted by multiplicative and impulsive noises," in *Proc. 8th European Signal Processing Conference (EUSIPCO '96)*, vol. 3, pp. 1909–1912, Trieste, Italy, September 1996.

[19] R. Touzi, "A review of speckle filtering in the context of estimation theory," *IEEE Trans. Geosci. Remote Sensing*, vol. 40, no. 11, pp. 2392–2404, 2002.

[20] V. P. Melnik, V. V. Lukin, A. A. Zelensky, J. T. Astola, and P. Kuosmanen, "Local activity indicators for hard-switching adaptive filtering of images with mixed noise," *Optical Engineering*, vol. 40, no. 8, pp. 1441–1455, 2001.

[21] J.-M. Park, W. J. Song, and W. A. Pearlman, "Speckle filtering of SAR images based on adaptive windowing," *IEE Proceedings—Vision, Image and Signal Processing*, vol. 146, no. 4, pp. 191–197, 1999.

[22] V. Melnik, *Nonlinear locally adaptive techniques for image filtering and restoration in mixed noise environments*, Ph.D. thesis, Tampere University of Technology, Tampere, Finland, 2000.

[23] V. V. Lukin, V. P. Melnik, A. B. Pogrebniak, A. A. Zelensky, J. T. Astola, and K. P. Saarinen, "Digital adaptive robust algorithms for radar image filtering," *Journal of Electronic Imaging*, vol. 5, no. 3, pp. 410–421, 1996.

[24] V. Lukin, N. Ponomarenko, J. T. Astola, and K. Saarinen, "Algorithms of image nonlinear adaptive filtering using fragment recognition by expert system," in *Nonlinear Image Processing VII*, vol. 2662 of *SPIE Proceedings*, pp. 179–190, San Jose, Calif, USA, January 1996.

[25] A. N. Dolia, A. Burian, V. V. Lukin, C. Rusu, A. A. Kurekin, and A. A. Zelensky, "Neural network application for primary local recognition and nonlinear adaptive filtering of images," in *Proc. 6th IEEE International Conference on Electronics, Circuits and Systems (ICECS '99)*, vol. 2, pp. 847–850, Pafos, Cyprus, September 1999.

[26] M.-P. Carton-Vandecandelaere, B. Vozel, L. Klaine, and K. Chehdi, "Application to multispectral images of a blind identification system for blur, additive, multiplicative and impulse noises," in *Proc. 11th European Signal Processing Conference (EUSIPCO '02)*, vol. 3, pp. 283–286, Toulouse, France, September 2002.

[27] S. K. Abramov, V. V. Lukin, A. A. Zelensky, and J. T. Astola, "Blind evaluation of noise variance in images using myriad operation," in *Image Processing: Algorithms and Systems*, vol. 4667 of *SPIE Proceedings*, pp. 192–203, San Jose, Calif, USA, January 2002.

[28] N. N. Ponomarenko, V. V. Lukin, S. K. Abramov, K. O. Egiazarian, and J. T. Astola, "Blind evaluation of additive noise variance in textured images by nonlinear processing of block DCT coefficients," in *Image Processing: Algorithms and Systems II*, vol. 5014 of *SPIE Proceedings*, pp. 178–189, Santa Clara, Calif, USA, January 2003.

[29] P. T. Koivisto, J. T. Astola, V. V. Lukin, V. P. Melnik, and O. V. Tsymbal, "Removing impulse bursts from images by training-based filtering," *Eurasip J. Appl. Signal Process.*, vol. 2003, no. 3, pp. 223–237, 2003.

[30] O. V. Tsymbal, V. V. Lukin, P. T. Koivisto, and V. P. Melnik, "Removal of impulse bursts in satellite images," in *Proc. 2nd IEEE International Workshop on Intelligent Data Acquisition and Advanced Computing Systems: Technology and Applications (IDAACS '03)*, pp. 324–329, Lviv, Ukraine, September 2003.

[31] Y. Yoshida and Y. Wu, "Classification of rotated and scaled textured images using invariants based on spectral moments," *IEICE Transactions on Fundamentals of Electronics, Communications and Computer Sciences*, vol. (E81-A), no. 8, pp. 1661–1666, 1998, Special section on digital signal processing.

[32] A. M. Akhmetshin and D. A. Mikhalev, "Classification of texture images with the usage of artificial neural nets and high-order statistics," in *Proc. 5th All-Ukrainian International Conference on Signal/Image Processing and Pattern Recognition (UkrObraz '00)*, pp. 173–176, Kyjiv, Ukraine, November–December 2000.

[33] J. C. Nunes, O. Niang, Y. Bouaoune, E. Delechelle, and Ph. Bunel, "Texture analysis based on the bidimensional empirical mode decomposition with gray-level co-occurrence models," in *Proc. 7th International Symposium on Signal Processing and Its Applications*, vol. 2, pp. 633–635, Paris, France, July 2003.

[34] S. C. Zhu, Y. Wu, and D. Mumford, "FRAME: filters, random fields, and minimax entropy towards a unified theory for texture modeling," in *Proc. IEEE Computer Society Conference on Computer Vision and Pattern Recognition (CVPR '96)*, pp. 686–693, San Francisco, Calif, USA, June 1996.

[35] A. Nieminen, P. Heinonen, and Y. Neuvo, "A new class of detail-preserving filters for image processing," *IEEE Trans. Pattern Anal. Machine Intell.*, vol. 9, no. 1, pp. 74–90, 1987.

[36] V. V. Lukin, A. A. Zelensky, N. N. Ponomarenko, A. A. Kurekin, J. T. Astola, and P. T. Koivisto, "Modified sigma filter with improved noise suppression efficiency and spike removal ability," in *Proc. 6th IEEE International Workshop on Intelligent Signal Processing and Communication Systems (ISPACS '98)*, pp. 849–853, Melbourne, Australia, November 1998.

[37] K. O. Egiazarian, V. P. Melnik, V. V. Lukin, and J. T. Astola, "Local transform-based denoising for radar image processing," in *Nonlinear Image Processing and Pattern Analysis XII*, vol. 4304 of *SPIE Proceedings*, pp. 170–178, San Jose, Calif, USA, January 2001.

[38] R. Oktem, *Transform domain algorithms for image compression and denoising*, Ph.D. thesis, Tampere University of Technology, Tampere, Finland, 2000.

[39] R. R. Coifman and D. L. Donoho, "Translation-invariant denoising," in *Wavelets and Statistics*, pp. 125–150, Springer, New York, NY, USA, 1995.

[40] L. Gagnon and A. Jouan, "Speckle filtering of SAR images: a comparative study between complex-wavelet-based and standard filters," in *Wavelet Applications in Signal and Image Processing V*, vol. 3169 of *SPIE Proceedings*, pp. 80–91, San Diego, Calif, USA, July 1997.

[41] V. V. Lukin, N. N. Ponomarenko, L. Y. Alekseyev, V. P. Melnik, and J. T. Astola, "Two-stage radar image despeckling based on local statistic Lee and sigma filtering," in *Nonlinear Image Processing and Pattern Analysis XII*, vol. 4304 of *SPIE Proceedings*, pp. 106–117, San Jose, Calif, USA, January 2001.

Oleg V. Tsymbal was born 1974 in Kharkov, Ukraine. He graduated from the National Aerospace University, Kharkov, Ukraine, and received Diploma of Computer Science and the Candidate of Technical Science degree in digital image processing in 1998 and 2003, respectively. He is currently completing his work toward the Doctor of Technology degree in Tampere International Center for Signal Processing, Tampere University of Technology, Tampere, Finland. His research interests include digital image processing and radar data interpretation.

Vladimir V. Lukin was born in 1960 in Belarus (FSU). He graduated in 1983 from the Faculty of Radioelectronic Systems, Kharkov Aviation Institute (now National Aerospace University), Kharkov, Ukraine, and received the Diploma with honors in radioengineering. Since then, he has been with the Department of Transmitters, Receivers, and Signal Processing at the same faculty. He received the Candidate of Technical Science degree in radioengineering, Senior Research Diploma, and the Doctor of Technical Science degree in 1988, 1991, and 2002, respectively. Since 1989, he has been Vice-Chairman of the Department of Transmitters, Receivers and Signal Processing. He has published more than 200 journal and conference papers in Ukraine, USA, Finland, Russia, and so forth. More than 80 of them are in English.

Nikolay N. Ponomarenko was born in 1970 in Kharkov, Ukraine. In 1993 he graduated from Kharkov Aviation Institute (now National Aerospace University, Kharkov, Ukraine) and Diploma in computer science. Since 1990, he has been with the Department of Transmitters, Receivers and Signal Processing, National Aerospace University. In 2004 he got Candidate of Technical Science degree in aerospace remote research. He is the author of more than 50 journal and conference papers. His area of interest includes remote sensing, digital signal image processing, and compression.

Alexander A. Zelensky was born in 1943 in Kharkov, Ukraine. He graduated from Kharkov Aviation Institute (now National Aerospace University, Kharkov, Ukraine) in 1966 and got the Diploma in radioengineering. Since that time he has beeen with the Faculty of Radioelectronic Systems, Kharkov Aviation Institute. He defended the Candidate of Technical Science thesis in 1972 and Doctor of Technical Science thesis in 1989. Since 1984 he has been the Chairman of the Department of Transmitters, Receivers, and Signal Processing. He is the author of more than 200 journal and conference papers as well as more than 100 patents. His research area includes digital signal/image processing and remote sensing.

Karen O. Egiazarian received the Ph.D. degree from Moscow M. V. Lomonosov State University, Russia, in 1986, and Doctor of Technology degree from Tampere University of Technology, Finland, in 1994. He is a leading scientist in signal, image, and video processing, with about 300 refereed journal and conference articles, three book chapters, and a book published by Marcel Dekker, Inc. His main interests are in the field of multirate signal processing, efficient algorithms, image and video denoising and compression, and digital logic. He is an Associate Editor of SPIE Journal of Electronic Imaging and a Member of the DSP Technical Committee of the IEEE Circuits and Systems Society.

Jaakko T. Astola received the Ph.D. degree in mathematics from Turku University, Finland, in 1978. From 1976 to 1977 he was with the Research Institute for Mathematical Sciences, Kyoto University, Kyoto, Japan. Between 1979 and 1987 he was with the Department of Information Technology, Lappeenranta University of Technology, Lappeenranta, Finland. In 1984 he worked as a Visiting Scientist at Eindhoven University of Technology, The Netherlands. From 1987 to 1992 he was Associate Professor in applied mathematics at Tampere University of Technology, Tampere, Finland. From 1993 he has been Professor of signal processing and Director of Tampere International Center for Signal Processing leading a group of about 60 scientists and was nominated Academy Professor by Academy of Finland (2001–2006). His research interests include signal processing, coding theory, spectral techniques, and statistics. He is a Fellow IEEE.